iScience

CellPress
OPEN ACCESS

Review

Application of metal-organic frameworks and their derivates for thermal-catalytic C1 molecules conversion

Shiyuan Lin,[1,3] Yongjie Chen,[1,3] Huayong Li,[1,3] Wenhang Wang,[1,2] Yang Wang,[1,*] and Mingbo Wu[1,*]

SUMMARY

One-carbon (C1) catalysis refers to the conversion of compounds with a single carbon atom, especially carbon monoxide (CO), carbon dioxide (CO_2), and methane (CH_4), into clean fuels and valuable chemicals via catalytic strategy is crucial for sustainable and green development. Among various catalytic strategies, thermal-driven process seems to be one of the most promising pathways for C1 catalysis due to the high efficiency and practical application prospect. Notably, the rational design of thermal-driven C1 catalysts plays a vital role in boosting the targeted products synthesis of C1 catalysis, which relies heavily on the choice of ideal active site support, catalyst fabrication precursor, and catalytic reaction field. As a novel crystalline porous material, metal-organic frameworks (MOFs) has made significant progress in the design and synthesis of various functional nanomaterials. However, the application of MOFs in C1 catalysis faces numerous challenges, such as thermal stability, mechanical strength, yield of MOFs, and so on. To overcome these limitations and harness the advantages of MOFs in thermal-driven C1 catalysis, researchers have developed various catalyst/carrier preparation strategies. In this review, we provide a concise overview of the recent advancements in the conversion of CO, CO_2, and CH_4 into clean fuels and valuable chemicals via thermal-catalytic strategy using MOFs-based catalysts. Furthermore, we discuss the main challenges and opportunities associated with MOFs-based catalysts for thermal-driven C1 catalysis in the future.

INTRODUCTION

In today's society, the manufacture of fuels and petrochemical commodities relies heavily on petroleum resources. However, due to the non-renewable nature of petroleum resources and the environmental pollution it brings, we urgently call for a cleaner and more sustainable way to synthesize fuels and petrochemical commodities. The utilization of compounds containing a single carbon atom (C1 molecules), such as CO, CO_2, and CH_4, for essential chemicals and clean fuels production possesses great potential for energy consumption upgrade and sustainable development.[1,2] The current main conversion pathways for C1 molecules into valuable chemicals and fuels are shown in Figure 1.[3] Syngas ($CO + H_2$) from the gasification of coal, biomass, and natural gas can be converted into platform chemicals (e.g., methanol, alkanes, and alkenes) via the direct pathway, as well as value-added products (e.g., aromatics, transportation fuels, light olefins, etc.) via the indirect process. It is obvious that the transformation of syngas can not only realize the clean utilization of coal and natural gas resources but also be employed as a bridging process to connect sustainable biomass resources and valuable products. Syngas conversion can also pave the way for the utilization of greenhouse gases CO_2 and CH_4 because these two greenhouse gases can be converted into syngas via the reverse water-gas shift reaction ($CO_2 + H_2 \rightarrow CO + H_2O$) and reforming strategy (dry reforming by CO_2, steam reforming by H_2O, and oxidative reforming by O_2), respectively. Additionally, C_{2+} hydrocarbons or oxygenates production from CO_2 hydrogenation, selective CH_4 oxidation, or CH_4 coupling opens a new window to eliminate the greenhouse gases in the atmosphere.

The highly efficient conversion of C1 molecules into valuable chemicals heavily relies on the catalysis strategy (denoted as C1 catalysis).[4,5] Due to the inert property of C-O or C-H bond in C1 molecules and sluggish behavior of C-C coupling during products synthesis, external energy (e.g., photo/thermal/electro-driven) should be added into the system to facilitate the C1 molecules transformation process. Among various strategies, the thermal-driven process seems to be more promising for practical application due to the high C1 molecules activation capability and targeted products yield.[6–8] Significant progress has been made in fundamental and applied research toward the development of C1 catalysis processes based on key catalytic systems. However, the current C1 conversion processes in the industry are characterized by high energy consumption and complicated procedures involving multi-step reactions and product separations, which encourages significant

[1]College of New Energy, College of Chemistry and Chemical Engineering, State Key Laboratory of Heavy Oil Processing, China University of Petroleum (East China), Qingdao 266580, China
[2]Shandong Provincial Key Laboratory of Chemical Energy Storage and Novel Cell Technology, School of Chemistry and Chemical Engineering, Liaocheng University, Liaocheng 252059, China
[3]These authors contributed equally
*Correspondence: wangyang@upc.edu.cn (Y.W.), wumb@upc.edu.cn (M.W.)
https://doi.org/10.1016/j.isci.2024.109656

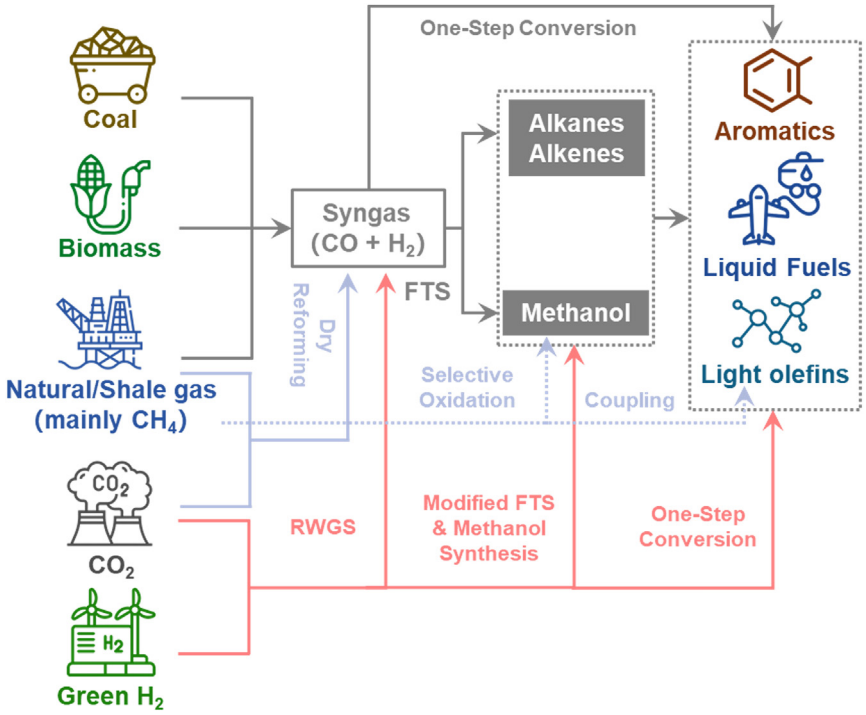

Figure 1. The conversion pathways for different C1 molecules to valuable chemicals
Reproduced with permission from Wang et al.[3] Copyright © 2023, American Chemical Society.

innovations in highly efficient catalyst design. Metallic catalysts with different scales, such as nanoparticles, clusters, and even single atoms, have been thoroughly investigated to realize the oriented conversion of C1 molecules into targeted products. The choice of ideal active site support, catalyst fabrication precursor, and even catalytic reaction field is essential to boost the catalytic performance of C1 catalysts.

Metal-organic frameworks (MOFs) have emerged as a highly promising new class of porous materials, which are composed of metal ions or clusters (also known as secondary building units, or SBUs) and bridging organic linkers.[9–12] Since the discovery, MOFs and MOFs-derived materials have garnered significant attention due to their remarkable features, including structural versatility and tunability,[13–17] low density,[18] high porosity,[19] and enormous specific surface area.[20] The unique characteristics of MOFs endow them as excellent support, precursor, and even reaction fields for the rational design of C1 catalysts. On the one hand, MOFs have unique and well-defined periodic crystal structures that allow for the uniform distribution of active sites throughout the framework. This feature facilitates efficient interactions between the catalyst and the substrates, resulting in a more uniform distribution of reaction intermediates and products. The tailorable porosity of MOFs further allows for the transportation of intermediates and products, therefore enhancing the overall reaction rate and selectivity. On the other hand, MOFs can serve as excellent templates/precursors to prepare various carbon/metal-based porous materials by means of pyrolysis. The obtained derivates inherit the characteristics of pristine MOFs to a large degree, such as large surface area, high porosity, composition diversity and dispersion, and excellent tailorability.

Under this background, MOFs have gained increasing attention from researchers as new catalytic materials for the transformation of C1 compounds, especially CO, CO_2, and CH_4. In recent years, significant progress has been made in the development of MOFs-based heterogeneous catalysts for the conversion of these C1 compounds. Many reviews on the conversion of CO, CO_2, and CH_4 to value-added chemicals with MOFs-based catalysts have been published.[21–25] In particular, Bu et al. reviewed studies of MOFs-based catalysts that catalyzed the conversion of CO, CO_2, and CH_4 to chemicals and clean fuels from the perspective of C1 chemistry in 2019.[26] The review highlighted the unique properties and advantages of these catalysts compared to traditional porous materials. It emphasized their potential for future research and development in this area. However, it should be noted that in recent years, numerous new advancements have been made in the primary and applied research of MOFs-based catalysts for the production of high-value chemicals via C1 catalysis. Accordingly, in this review, we briefly summarize the latest achievements of MOFs-based catalysts in the conversion of C1 molecules (mainly including CO, CO_2, and CH_4) into valuable chemicals via thermal-catalytic strategy, as illustrated in Figure 2. By outlining these examples, we aim to provide a comprehensive understanding of the progress made in this field and the potential of MOFs-based C1 catalysts for future research and practical application.

CO CONVERSION

Carbon monoxide is a colorless, odorless, and tasteless gas, highly toxic, and primarily produced through partial oxidation or incomplete combustion of carbon-containing compounds. From an environmental perspective, CO is an atmospheric pollutant, necessitating its removal

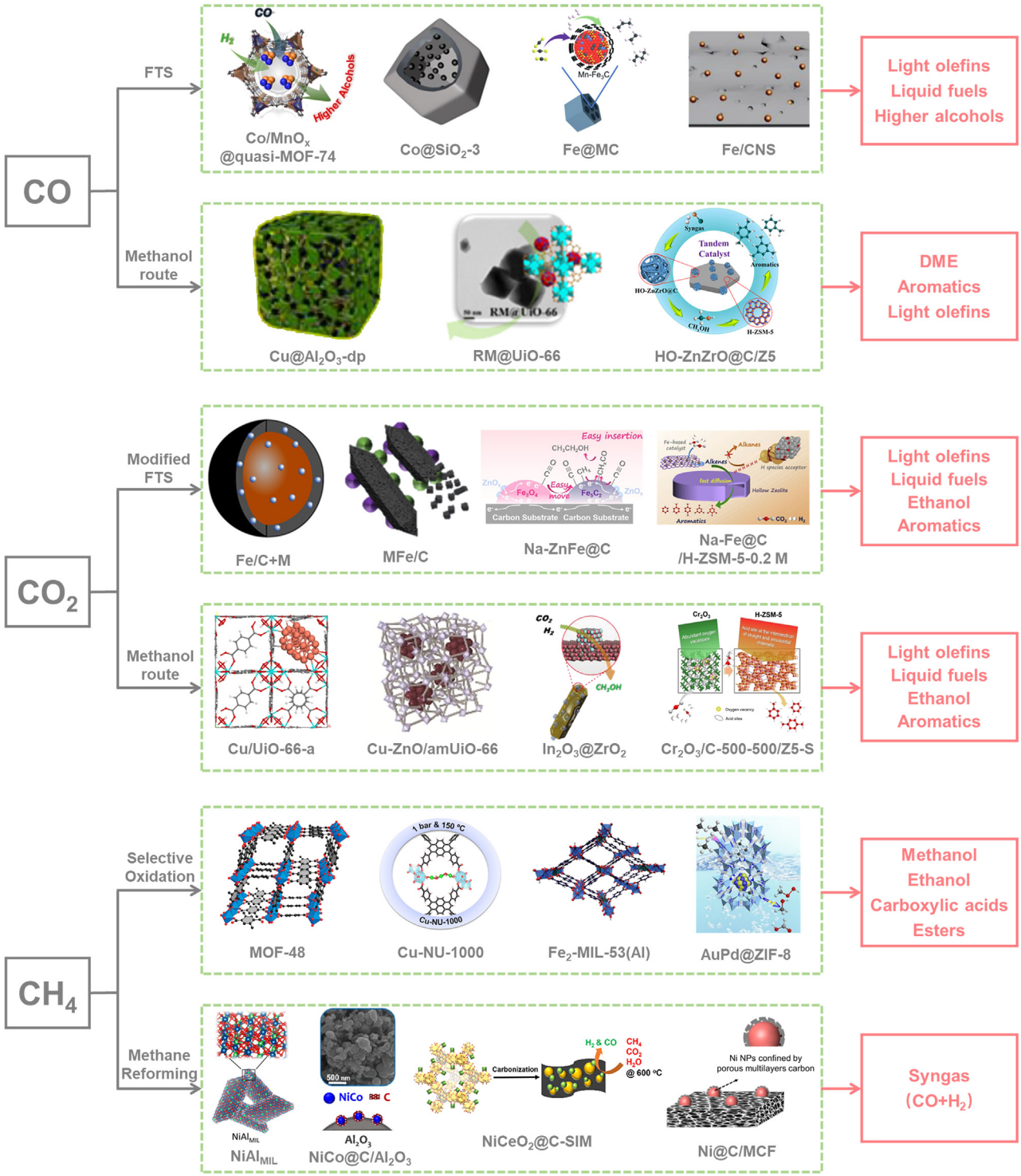

Figure 2. C1 molecules to valuable chemicals via MOFs-based catalysts

through catalytic oxidation in applications such as automotive emission control and air purification.[27,28] Conversely, from the standpoint of energy security and industrial production, CO holds immense value as a primary chemical raw material for valuable chemicals and liquid fuels production. CO comes from a wide range of sources and can be produced from coal, biomass and organic waste gasification, or methane (CH_4) conversion. The main product of these production processes is synthesis gas (CO + H_2), which can be used directly as a chemical

feedstock to produce clean fuels and value-added chemicals. By converting natural gas, coal, biomass, and other non-petroleum carbon resources into high-value-added chemicals and clean fuels, an attractive alternative non-petroleum pathway is provided for the production of hydrocarbons. There are two main routes for syngas conversion, namely the Fischer-Tropsch Synthesis (FTS) and methanol routes. Fischer-Tropsch Synthesis (FTS) refers to the conversion of syngas (CO + H_2) into hydrocarbon fuels and chemicals by adsorption and activation of CO/H_2 and C-C coupling in the presence of a metal catalyst.[6,29–31] On the other hand, syngas can be converted to the critical intermediate methanol on suitable catalysts (usually copper-based or reducible metal oxide) in the methanol route. The resulting methanol can be further converted to compounds such as dimethyl ether (DME), light olefins, aromatics etc., in the presence of acid catalysts (mainly zeolites). The syngas-to-methanol route tends to involve more complex catalytic systems and reaction conditions.[32–35]

This section focuses on the conversion of CO to high-value chemicals via FTS and methanol routes using MOFs and their derivates as catalysts or carriers.

MOFs-based catalysts for FTS

The FTS process requires demanding reaction conditions. Limited by relatively low thermal, hydrothermal, and chemical stability, pristine MOFs usually cannot perform well in FTS. In order to overcome this limitation, the study of MOFs-derived catalysts, the synthesis of carbon-based materials with unique structures by high-temperature pyrolysis using pristine MOFs as templates and/or precursors, has recently become a hot spot. The obtained MOFs-derived materials retain some of the specific properties of MOFs-precursors and can also be adapted to the reaction conditions of FTS.[36,37] In this review, we focus on two types of FTS catalysts reported so far: Fe-MOFs-derived FTS catalysts and Co-MOFs-derived FTS catalysts. The catalytic activities of MOFs-based catalysts for FTS reported in recent years are summarized in Table 1.

Co-MOFs derived FTS catalysts

In 2016, Isaeva et al. prepared novel nanohybrid materials by immobilizing cobalt nanoparticles on a microporous framework, MIL-53(Al), which serves as a porous host matrix. The catalytic properties of Co@MIL-53(Al) nanohybrids were investigated in Fischer-Tropsch Synthesis (FTS).[38] For MOFs materials, structural stability and suitable active sites are essential for achieving a high C_{2+}OH selectivity in FTS.[21] However, these MOFs-derived materials usually have a lower surface area and collapsed skeletal structure after high-temperature decomposition, resulting in a large amount of active metal sites being embedded into the bulk phase and coated with graphite carbon.[36,37] Hu et al. constructed a core-shell Co/MnO_x@quasi-MOF-74 catalyst by controlling the delocalization of bimetallic CoMn-MOF-74 through a partial pyrolysis strategy, which largely preserved the original skeleton of MOFs and generated many highly active Co/MnO_x nanoparticles *in situ*.[39] At 200°C, 3.0 MPa (CO/H_2 = 1/2) and 4500 mL g^{-1} h^{-1} of GHSV, the alcohol selectivity reached 48.7 wt %, of which 93.1 wt % was C_{2+} alcohols. Mechanistically, the porosity and skeletal structure of the core-shell catalysts ensured that the reactants were able to diffuse into the active sites even though Co^0, Co^{2+}, and Co_2C, where the metal Co was used for CO dissociation and chain growth of the C_{2+} alkyl chains, while the CUS of Co^{2+} and Co_2C were used for CO insertion to generate C_{2+}OH (Figure 3). Luo et al. reported a strategy for the preparation of highly dispersed Co-embedded porous carbon nanocage (CoPCN) structures derived from ZIF-8@ZIF-67 precursor.[40] By pyrolyzing the core-shell ZIF-8@ZIF-67 precursor at high temperatures, the metallic zinc in the ZIF-8 core was vaporized by high-temperature pyrolysis to form the nanocages, which resulted in the formation of a well-developed porous structure and the realization of high Co loading with a weight percentage of more than 30%. The porous channels and hollow structure of CoPCN enhanced the diffusion of reactants and hydrocarbon products and improved the selectivity of C_{5+} and CO conversion.

The presence of graphitic carbon layers after pyrolysis can cover the active sites and inhibit the adsorption and activation of reactants, resulting in a decrease in the FTS activity of the catalyst. Calcination of Co@C catalysts in air removes the graphitic carbon layer, but without the constraining effect of the carbon skeleton, the Co particles will be agglomerated, thus inducing catalyst deactivation.[41–43] Therefore, some researchers have worked on improving the FTS performance of MOFs-derived catalysts through the role of a cladding hydrophobic layer or the support. Li et al. prepared Co@C catalysts using zeolite imidazolium hydrochloride framework-67 with MOFs structure as precursors with high cobalt loading of 55.6 wt % and small cobalt crystal size of 8.6 nm.[44] Co@C@SiO_2-X core-shell catalysts with different SiO_2 shell thicknesses were successfully prepared by coating different amounts of TEOS (tetraethyl orthosilicate) on the outer surface of Co@C to change the product selectivity. In follow-up research, Li et al. used an *in situ* doping method to introduce an aluminum source during the synthesis of ZIF-67 to obtain a high-performance Co_3O_4/Al_2O_3-x catalyst.[45] The effects of different Al precursors (including $AlCl_3 \cdot 6H_2O$, $Al(C_3H_7O)_3$, and Al $(NO_3)_3 \cdot 9H_2O$) on the catalytic performance were also investigated. The prepared Co_3O_4/Al_2O_3-x catalysts showed better FTS activity and lower CH_4 selectivity than the Co@C catalysts obtained by direct carbonization. The Co_3O_4/Al_2O_3-x catalysts with different aluminum sources showed different FTS performances, among which the catalysts using Al $(NO_3)_3 \cdot 9H_2O$ as the aluminum source showed the best performance, with stronger metal-support interactions, smaller Co particle sizes, and a higher number of active sites. Ding et al. synthesized a hollow Co@SiO_2 catalyst with cobalt species highly dispersed within a mesoporous hollow silica shell with the help of cobalt MOFs materials (Figure 4), which showed a high selectivity of 93.3% for C_{5+} hydrocarbons and only 3.4% for CH_4.[46] Compared with conventional encapsulated catalysts, the hollow core-shell structure provided an inner-cavity environment, which shortened the diffusion distance and contact area between cobalt metal and support. It improved the residence time of the exposed active cobalt sites and intermediates, thus enhancing the catalytic activity and the selectivity for long-chain hydrocarbons. Using natural macro-porous wood combined with microporous MOFs, Jiang et al. prepared Co@C/CW, a monolithic 3D catalyst for Fischer-Tropsch synthesis application, by growing Co-MOF *in-situ* on a wood monolith and carbonizing it.[47] In general, Co@C/CW showed higher CO conversion and C_{5+} selectivity, attributed to its 3D

Table 1. Summary of the catalytic performance of MOFs-derived FTS catalysts reported in recent years

Entry	Catalyst	T (°C)	P (MPa)	GHSV[a] (mL g_{cat}^{-1} h^{-1})	H_2/CO	X_{CO} (%)	S_{CO2} (%)	S_{CH4} (%)	Desired product (%)	Reference
1	Co/MnO_x@quasi-MOF-74	200	3.0	4500	2	6.7	0.0	3.4	45.4 of S_{ROH}, 93.1 of C_{2+}OH/ROH	Cui et al., 2020[39]
2	Co/MnO_x@quasi-MOF-74	220	3.0	4500	2	12.1	0.0	7.0	42.4 of S_{ROH}, 92.5 of C_{2+}OH/ROH	Cui et al., 2020[39]
3	Co/MnO_x@quasi-MOF-74	230	3.0	4500	2	21.4	0.8	10.0	39.0 of S_{ROH}, 92.1 of C_{2+}OH/ROH	Cui et al., 2020[39]
4	CoPCN-920	220	2.5	5300	2	18.3	–	10.9	8.9 of S_{C2-C4}, 80.2 of S_{C5+}	Lü et al., 2020[40]
5	ZIF-67-920	220	2.5	5300	2	4.8	–	4.8	29.4 of S_{C2-C4}, 28.6 of S_{C5+}	Lü et al., 2020[40]
6	Co@C@SiO_2-0	230	2.0	6750	2	35.6	2.1	26.1	11.0 of S_{C2-C4}, 62.9 of S_{C5+}	Chen et al., 2020[44]
7	Co@C@SiO_2-1	230	2.0	6750	2	29.2	1.4	22.2	11.9 of S_{C2-C4}, 65.9 of S_{C5+}	Chen et al., 2020
8	Co@C@SiO_2-2	230	2.0	6750	2	22.2	1.0	17.3	8.6 of S_{C2-C4}, 74.1 of S_{C5+}	Chen et al., 2020
9	Co@C@SiO_2-4	230	2.0	6750	2	13.3	1.0	15.7	6.7 of S_{C2-C4}, 77.6 of S_{C5+}	Chen et al., 2020
10	Co_3O_4/Al_2O_3-I	230	2.0	12($SL \cdot g^{-1} \cdot h^{-1}$)	2	35.5	0.3	7.9	4.4 of S_{C2-C4}, 87.7 of S_{C5+}	Zhao et al., 2021[45]
11	Co_3O_4/Al_2O_3-II	230	2.0	12($SL \cdot g^{-1} \cdot h^{-1}$)	2	33.5	0.3	7.6	4.1 of S_{C2-C4}, 88.3 of S_{C5+}	Zhao et al., 2021[45]
12	Co_3O_4/Al_2O_3-III	230	2.0	12($SL \cdot g^{-1} \cdot h^{-1}$)	2	62.6	1.3	12.3	5.9 of S_{C2-C4}, 81.8 of S_{C5+}	Zhao et al., 2021[45]
13	Co@SiO_2-3	210	2.0	17500	1	49.2	1.2	3.4	93.1 of S_{C5+}	Qin et al., 2022[46]
14	Co@SiO_2-3	210	2.0	17500	2	98.3	1.3	7.0	89.9 of S_{C5+}	Qin et al., 2022[46]
15	Co@C/CW-100	240	2.0	10000	2	92.6	–	~12.0	~30.0 of S_{C2-C4}, 58.1 of S_{C5+}	47
16	Co@C/CW-100	240	2.0	40000	2	89.6	–	~13.0	~32.5 of S_{C2-C4}, 53.5 of S_{C5+}	Qin et al., 2021[47]
17	Co@C/CW-100	240	2.0	50000	2	81.2	–	~22.5	~35.0 of S_{C2-C4}, 48.5 of S_{C5+}	Qin et al., 2021[47]
18	CoPNP-600	220	2.5	5300	2	71.6	<6.0	22.0	12.1 of S_{C2-C4}, 65.9 of S_{C5+}	Luo et al., 2021[51]
19	CoPNP-700	220	2.5	5300	2	62.5	<6.0	14.5	15.3 of S_{C2-C4}, 70.2 of S_{C5+}	Luo et al., 2021[51]

(*Continued on next page*)

Table 1. *Continued*

Entry	Catalyst	T (°C)	P (MPa)	GHSV[a] (mL g_{cat}^{-1} h^{-1})	H_2/CO	X_{CO} (%)	S_{CO2} (%)	S_{CH4} (%)	Desired product (%)	Reference
20	CoPCN-920	220	2.5	5300	2	18.3	<6.0	10.9	8.9 of S_{C2-C4}, 80.2 of S_{C5+}	Luo et al., 2021[51]
21	Co4.7Mo@C	275	3.0	15000	2	48.0	–	–	19.7 of S_{MeOH} 80.3 of S_{C2+OH}	54
22	CoMn-350	240	3.0	3750	2	51.5	0.5	7.7	57.5 of S_{ROH}, 47.4 of S_{C2+OH}	Guo et al., 2023[55]
23	FeC(4,700)	300	2.0	8000	~2	88.9	34.4	8.9	15.4 of S_{C2-C4}, 75.7 of S_{C5+}	Cho et al., 2020[60]
24	FeC(4,800)	300	2.0	8000	~2	84.6	32.8	8.9	16.3 of S_{C2-C4}, 74.8 of S_{C5+}	Cho et al., 2020[60]
25	FeC(4,900)	300	2.0	8000	~2	73.1	31.8	10.8	17.6 of S_{C2-C4}, 71.6 of S_{C5+}	Cho et al., 2020[60]
26	Fe-MIL-88B-T/C	280	2.0	4200	1	94	43.0	17.0	40 of S_{C2-C4}, 43 of S_{C5+}	Rashed et al., 2022[61]
27	R-1	300	2.0	36000	1	14.1	7.5	4.2	10.41 of S_{C2-C4}, 85.36 of S_{C5+}	Mehar et al., 2020[62]
28	R-2	300	2.0	36000	1	12.2	8.2	8.2	13.03 of S_{C2-C4}, 81.79 of S_{C5+}	Mehar et al., 2020[62]
29	R-3	300	2.0	36000	1	8.0	5.4	5.4	9.59 of S_{C2-C4}, 86.36 of S_{C5+}	Mehar et al., 2020[62]
30	R-4	300	2.0	36000	1	5.2	6.8	5.2	12.78 of S_{C2-C4}, 82.06 of S_{C5+}	Mehar et al., 2020[62]
31	R-5	300	2.0	36000	1	5.4	4.0	3.3	8.56 of S_{C2-C4}, 88.19 of S_{C5+}	Mehar et al., 2020[62]
32	Fe/CNS(900)	340	1.0	9000	1	33.9	31.9	26.5	28.4 of S_{C2-C4}, 28.4 of S_{C5+}	Zhao et al., 2021[66]
33	Fe/CNS(950)	340	1.0	9000	1	40.2	32.2	24.3	23.2 of S_{C2-C4}, 35.6 of S_{C5+}	Zhao et al., 2021[66]
34	Fe/CNS(1000)	340	1.0	9000	1	51.2	33.0	23.6	22.0 of S_{C2-C4}, 36.3 of S_{C5+}	Zhao et al., 2021[66]
35	Fe/CNS(1100)	340	1.0	9000	1	31.0	31.2	28.4	23.0 of S_{C2-C4}, 31.6 of S_{C5+}	Zhao et al., 2021[66]
36	Fe@C	340	2.5	5000	1	27.0	20.0	17.0	20 of S_{C2-C4}, 63 of S_{C5+}	Wang et al., 2021[68]
37	Na/Fe@C	340	2.5	5000	1	51.0	34.0	16.0	18 of S_{C2-C4}, 66 of S_{C5+}	Wang et al., 2021[68]

(*Continued on next page*)

Table 1. *Continued*

Entry	Catalyst	T (°C)	P (MPa)	GHSV[a] ($mL\ g_{cat}^{-1}\ h^{-1}$)	H_2/CO	X_{CO} (%)	S_{CO2} (%)	S_{CH4} (%)	Desired product (%)	Reference
38	Cu/Fe@C	340	2.5	5000	1	91.0	40.0	29.0	36 of S_{C2-C4}, 35 of S_{C5+}	Wang et al., 2021[68]
39	Ru/Fe@C	340	2.5	5000	1	60.0	35.0	41.0	30 of S_{C2-C4}, 29 of S_{C5+}	Wang et al., 2021[68]
40	Fe@C	340	2.5	5000	1	94.0	42.0	22.0	36 of S_{C2-C4}, 42 of S_{C5+}	Wang et al., 2022[69]
41	FeCo@C	340	2.5	5000	1	99.0	40.0	40.0	29 of S_{C2-C4}, 31 of S_{C5+}	Wang et al., 2022[69]
42	FeNi@C	340	2.5	5000	1	87.0	40.0	53.0	17 of S_{C2-C4}, 30 of S_{C5+}	Wang et al., 2022[69]
43	FeMn@C	340	2.5	5000	1	73.0	40.0	18.0	31 of S_{C2-C4}, 51 of S_{C5+}	Wang et al., 2022[69]
44	FeZn@C	340	2.5	5000	1	94.0	42.0	28.0	34 of S_{C2-C4}, 38 of S_{C5+}	Wang et al., 2022[69]

[a]Gas hourly space velocity.

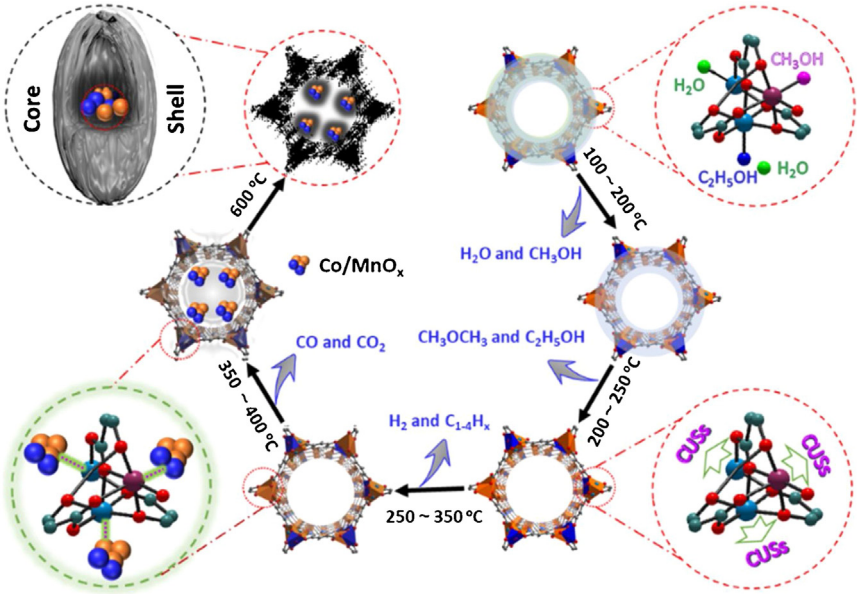

Figure 3. Schematic illustration of the calcination-induced structure changes of the CoMnMOF-74
Reproduced with permission from Cui et al.[39] Copyright © 2020, Elsevier.

multi-channel reactor structure and more contact surfaces. In the three-dimensional structure of tracheal cells, Co-MOF was well separated, yielding more contact surfaces. In addition, the mesoporous structure of Co@C/CW-100 facilitates the diffusion, adsorption, reaction, and dissociation of synthesis gas on the Co@C surface, resulting in higher C_{5+} selectivity.

The impregnation method is widely used to prepare industrial FTS catalysts, often yielding Co loadings below 20 wt %. At the same time, the support usually has strong metal-support interactions with the Co species, leading to irreversible catalyst deactivation.[48–50] Layered double hydroxide (LDH) is a typical inorganic layered substrate, and active Co can be used as a component of the LDH substrate to achieve higher metal loadings. Lv et al. prepared ZIF-67 MOFs grown *in situ* on CoAl LDH and subsequently prepared highly dispersed Co-embedded porous nanoparticle (CoPNP) catalysts for FTS by pyrolysis.[51] The CoPNP showed a hierarchical structure with a high specific surface area. The CoPNP showed a hierarchical structure with a high specific surface area, and the porous channels could enhance syngas diffusion and hydrocarbon production and improve CO conversion and C_{5+} selectivity, with CO conversion up to 71.6% and C_{5+} long-chain hydrocarbon selectivity up to 70.2% (Figure 5). Due to the unsaturated coordination state provided by the Co cation on the LDH surface, ZIF-67 can be grown *in situ* on the LDH surface to form CoAl-LDH/ZIF-67. The pyrolysis of CoAl-LDH/ZIF-67 mainly leads to two structural transformations: the transformation of the ZIF-67 crystals into porous graphitic carbon and the transformation of CoAl-LDH nanoparticles into Co nanoparticles.

Recently, the selective conversion of syngas to higher alcohols (HA) has been of great interest. Modified Co-based catalysts have attracted much attention due to their excellent activity, relatively high HA selectivity, and low water-gas shift capability.[52,53] Wang et al. reported a special MOFs-assisted strategy to prepare well-contained Co-Mo bimetallic refiners based on MOFs pyrolysis, with an optimal ratio of Co^0 and Co_6Mo_6C to $Co_{4.7}Mo$@C at 275°C and 3.0 MPa, which resulted in a 48% CO conversion and a C_{2+}OH time space yield (STY) of 99 mg g_{cat}^{-1} h^{-1}.[54] Ma et al. prepared a series of catalysts by partially thermally decomposing CoMn-MOF materials with layered structures.[55] The MOFs framework could be partially retained after calcination at 350°C under nitrogen flow, where Co^{2+} species could provide additional non-dissociatively adsorbed CO sites, thus improving alcohol selectivity. The addition of manganese promotes cobalt dispersion and Co_2C formation. The synergistic catalytic effect of these actives resulted in higher selectivity of the optimal CoMn-350 catalyst for higher alcohols.

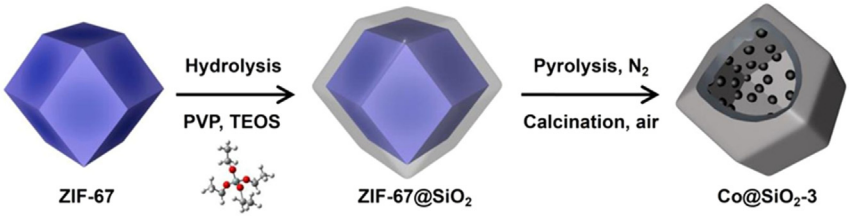

Figure 4. Illustration of the synthesis of hollow Co@SiO$_2$-3 catalyst
Reproduced with permission from Qin et al.[46] Copyright © 2022, Elsevier.

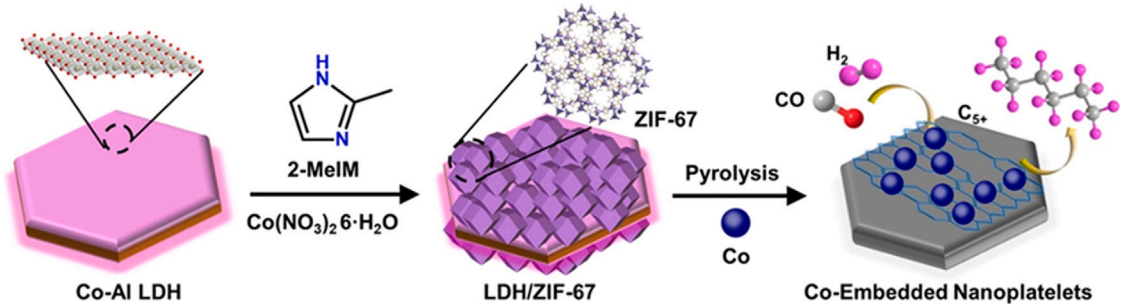

Figure 5. Schematic of the preparation of CoPNP catalysts and the production of C_{5+} long-chain hydrocarbons from syngas
Reproduced with permission from Luo et al.[51] Copyright © 2021, American Chemical Society.

Fe-MOFs derived FTS catalysts

Fe-based catalysts have been widely studied among active transition metals of all types due to their low market cost, easy availability, high water gas shift activity (WGS), flexible product distribution, and tunable engineering properties.[56,57] For Fe-MOFs materials, the different porosities, and thicknesses of the carbon layers, as well as the particle sizes of the metal nanoparticles, can be easily adjusted by adjusting the pyrolysis conditions to preferentially form highly dispersed smaller metal nanoparticles from the MOFs with a crystalline phase suitable for the FTS reaction.[58,59] Jong et al. applied iron carbide catalysts derived from MIL-100(Fe) MOFs to the Fischer-Tropsch synthesis reaction by direct pyrolysis, and the obtained iron carbides were easy to form active iron carbide phases due to the small grain size of the obtained iron carbides.[60] The crystallite sizes of metallic Fe and Fe_3O_4 on FeC increased with increasing pyrolysis temperature (700°C–900°C) and duration (4 h–16 h). Based on the similar pore volume and pore size on FeC, the catalytic activity is closely related to the specific surface area and crystallite size of FeC nanoparticles, and smaller FeC nanoparticles with larger specific surface area and thinner carbon layer seem to allow easier access of reactants to the active sites and thus higher catalytic activity. Ahmed et al. used TEA instead of NaOH as a deprotonation catalyst to synthesize Fe-MIL-88B MOFs, which improved the synthesis yield of MOFs and was conducive to forming smaller crystals.[61] Smaller crystals result in higher activity and olefins yield.

Catalyst pretreatment is another crucial step during the FTS process, which involves catalyst reduction under different reduction atmospheres seeking an active catalyst. Li et al. investigated the effects of different reduction atmospheres on the FTS reaction products of MOFs-derived Fe-based catalysts, revealing a close relationship between reduction atmospheres and FTS catalytic activity (Figure 6).[62] The reduction atmospheres mainly affected the FTS catalytic activity. At the same time, they had little effect on the product selectivity, where the catalysts reduced in a pure CO atmosphere had the highest CO conversion. In contrast, the catalysts reduced with H_2 and syngas had a more stable reaction but lower activity and a higher C_{5+} selectivity. Li et al. investigated the synthesis of Fe@C catalysts by direct pyrolysis of FeMIL-88B with the structure of MOFs at different elevated temperatures (600, 700, and 800°C), which overcame the problem that the high C_{5+} selectivity usually comes at the cost of lower CO conversion. The catalyst Fe@C-800 decomposed at 800°C showed a very high C_{5+} hydrocarbon selectivity close to 90% and good reaction stability. MOFs-derived Fe-based catalysts have the potential to achieve high C_{5+} selectivity for FTS without lowering the CO conversion.

Functionalizing carbon supports with heteroatom doping is known as one type of chemical modification strategy. The framework N atoms, as electronic donors, can enhance the electron density of adjacent metal species and help anchor metal species by strengthening metal

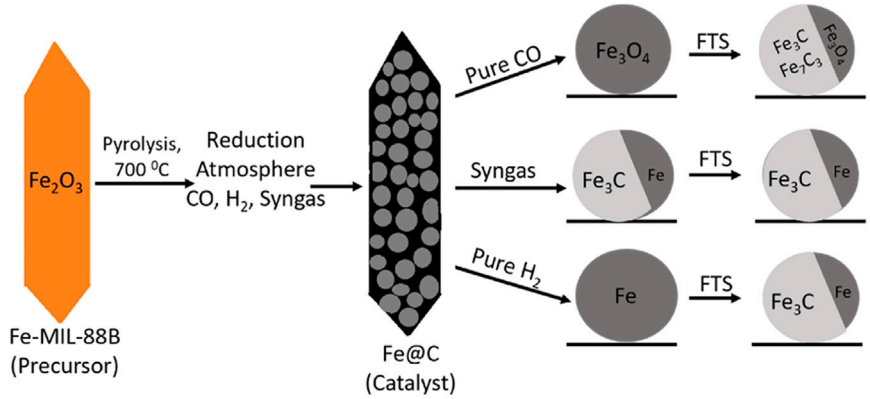

Figure 6. Schematic diagram displaying phase transformation over reduction and FTS reaction
Reproduced with permission from Nisa et al.[62] Copyright © 2019, Elsevier

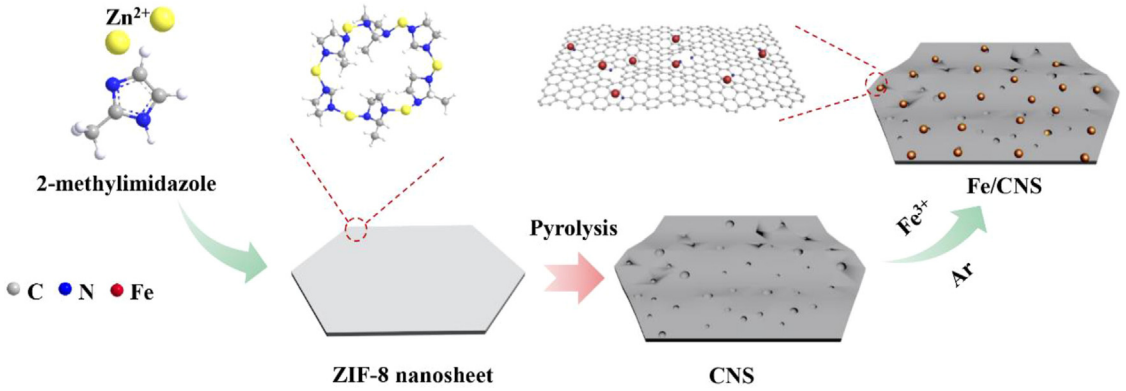

Figure 7. Schematic illustration of the synthesis process for preparing Fe/CNS catalyst
Reproduced with permission from Zhao et al.[66] Copyright © 2020, Elsevier

support interactions, improving metal dispersion and sintering resistance.[63–65] Ma et al. used a MOFs-derived class of Fe-based catalysts, and the derived CNS exhibited a higher degree of graphitization and electronic effects to promote Fe carburization, thereby enhancing the intrinsic activity of the catalysts in FTS (Figure 7).[66] Furthermore, a comparison of the Fe/CNS, Fe/CP, and Fe/AC catalysts reveals that MOFs morphology and N doping significantly affect the CO conversion, and N doping also affects the product distribution. The MOFs-derived N-doped carbon nanosheets as supports show significant advantages in FTS due to their unique morphology and the electronic effect of N species. The presence of sulfur caused pores to form inside the particles during the catalyst preparation. This phenomenon has also sparked the interest of researchers. Iqbal et al. found that the presence of sulfur in $Fe_2(SO_4)_3$ MOFs provided a significant amount (52.50%) of light hydrocarbons in the carbon chain distribution.[67] High-temperature annealing made the pores of the MOFs finer, improving the catalytic products' selectivity. High-temperature pyrolysis during catalyst preparation brought iron and carbon into contact more rapidly and promoted the formation of the active phase of iron carbide. Characterized by SEM, the MOFs prepared from iron sulfate showed sulfur particles attached to iron and carbon particles. The presence of sulfur particles decreased after calcination under the tube furnace atmosphere due to the reaction of sulfur with free water molecules to generate heat, leading to the formation of pores inside the particles.

Additionally, adding alkali and other metallic promoters to Fe-based FTS catalysts is a good choice for improving catalytic activity, selectivity, and stability. Transition metals can be used as electronic and structural promoters in FeO_x-FeC_x catalysts and concurrently alter the active site distribution. Luo et al. investigated the Fischer-Tropsch synthesis of porous carbon-loaded Fe-based catalysts based on MOFs promoted by Na, Cu, and Ru metals.[68] Among them, the Cu sample showed the best activity promotion (FTY = 0.154 mol CO g_{Fe}^{-1} h^{-1}), the Ru sample showed more than 70% selectivity for C_{1-4} hydrocarbons, and the Na sample showed the highest C_{5+} selectivity of 66%. XRD and TEM characterization confirmed that the enhancement of FTS activity and selectivity of the promoted catalysts was related to the reduction of Fe particle size, which improved the FTS performance by stabilizing the small-sized Fe nanoparticles on the surface of the carbon matrix and preventing their further aggregation at high temperature. In follow-up research, Luo et al. synthesized a bimetallic MOFs, FeM-MOF-74.[69] Then, they prepared bimetallic FT catalysts with high metal loading (Fe+M > 50 wt %) and uniformly dispersed active sites by pyrolysis of bimetallic MOFs. Among them, FeCo@C showed the highest CO conversion, FeMn@C showed a trend toward light olefins, and FeZn@C produced the highest FTY. The bimetallic catalysts showed higher activity compared to the monometallic Fe catalysts. With the addition of Mn, the olefin to paraffin ratio of Fe@C and FeMn@C catalysts was significantly increased from 0.43 to 1.23, the selectivity of long-chain hydrocarbons (C_{5+}) was increased from 42% to 51%, and the CH_4 generation was suppressed from 22% to 18%. This behavior can be explained by the electronic effect of Mn species, which can change the valence state of adjacent Fe and promote the dissociation of CO.

In summary, both Fe-MOFs and Co-MOFs belong to MOF materials with a highly ordered pore structure, which can be adjusted regarding pore size and functionality by selecting different organic ligands and metal centers. However, due to the different metal centers, the differences in the electronic structure and surface properties of their active centers lead to different activities and selectivity in the catalytic reactions. Fe-based materials usually have higher conversion rates for CO and tend to produce more olefins and oxides (e.g., CO_2), while Co-based catalysts have relatively lower reaction temperatures and produce more saturated hydrocarbons. In practical industrial applications, the selection of a suitable catalyst needs to be based on the reaction conditions, the desired product distribution, and the requirements for catalyst stability.

MOFs-based catalysts for methanol route of CO conversion

In addition to FTS, syngas can be used to synthesize high-value chemicals via the methanol route. Research on the one-step conversion of syngas to high-value chemicals via a methanol intermediate route through efficient catalysts is attracting the interest of researchers.[32–35] DME production has traditionally been realized via a two-step process, where methanol is synthesized from syngas and then dehydrated to DME. Compared with the two-step synthesis of DME, the direct one-step syngas-to-DME (STD) reaction breaks the thermodynamic

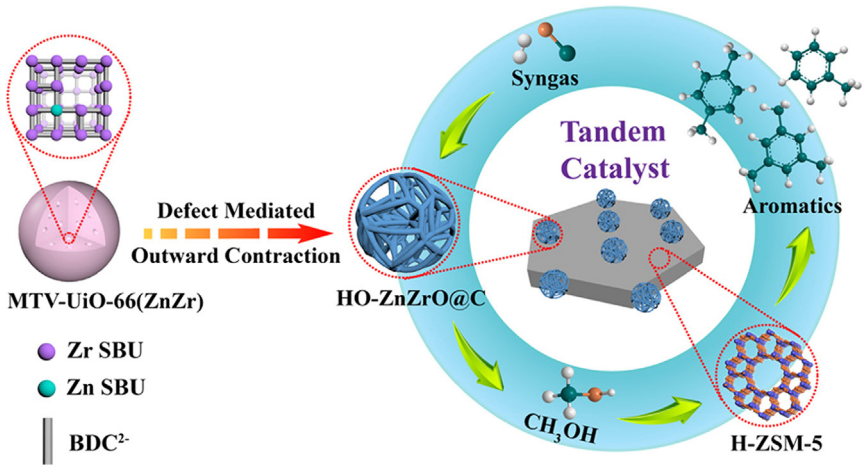

Figure 8. Fabrication Strategy of HO-ZnZrO@C and reaction process for direct production of aromatics from syngas over HO-ZnZrO@C/Z5
Reproduced with permission from Wang et al.[73] Copyright © 2020, American Chemical Society.

equilibrium limitation of methanol synthesis from syngas.[70–72] The high DME synthesis performance heavily relies on the well-organized structure of the catalysts. MOFs have received increasing attention from researchers worldwide due to their regular crystal structure and well-developed porosity.[33] Liu et al. prepared Cu/ZnO catalysts with a novel octahedral structure by two-step pyrolysis of Zn-doped Cu-BTC MOFs via one-pot solvothermal and two-step calcination methods.[32] The homogeneous distribution of Cu and Zn in the unique octahedral morphology significantly reduces the aggregation and migration of the Cu0 nanoparticles, which enhances the activity and stability of DME production. In addition, the partial reduction of ZnO led to the formation of Cu^{+}-O-Zn, further promoting the DME production and showing the best DME generation activity (7.74% CO conversion and 70.05% DME selectivity) after 40 h of continuous reaction. Zhao et al. successfully prepared a new type of Cu-embedded porous Al_2O_3 catalyst by filling $Al(OH)_3$ into a Cu-BTC skeleton via a deposition-precipitation-calcination process.[33] The prepared Cu@Al_2O_3-dp catalyst has a unique embedded structure with higher Cu dispersion, and the CO conversion and DME selectivity in the STD reaction reached 25.7% and 90.4%, respectively, with higher product selectivity and stability than that of the pure Al_2O_3 supported Cu catalyst.

Aromatics are mainly produced from petroleum refining and are essential basic chemicals. It is extremely attractive to utilize MOFs and their derivative materials to build ingenious structures at the molecular level and develop efficient catalysts with desirable properties for hydrogenating CO to aromatics with high activity and selectivity. Li et al. explored a facile "defect-mediated outward shrinkage" strategy using a Zr geometry to replace Zn in MTV-UiO-66 (Figure 8).[73] Subsequently, they carbonized to prepare a robust 3D layered carbon framework and ultrafine metal oxide nanoparticles capable of delivering abundant surface oxygen vacancies, a higher density of exposed active sites, and open and continuous channels. And by coupling with layered H-ZSM-5, the tandem catalyst HO-ZnZrO@C/Z5-0.6 was obtained with aromatic selectivity (73.1%) and lower CH_4 selectivity (3.4%), as well as up to 0.302 g g_{oxide}^{-1} h^{-1} aromatic STY at a CO conversion of 35.2%.

Coal or biomass-based light olefin production routes include methanol to olefin (MTO) based on synthesis of syngas and Fischer-Tropsch synthesis of olefins (FTO). FTO is difficult to achieve high light olefins selectivity due to the Anderson-Schuler-Flory (ASF) distribution.[74,75] MTO has emerged as the alternate pathway for supplying light olefins. Ying et al. prepared $ZnZrO_x$ nanoparticles by MOFs calcination, and the XPS results showed that the MOFs-derived $ZnZrO_x$-400 had more oxygen vacancies and Zn-O-Zr structures.[34] CO-TPD and *in situ* DRIFTS indicated that $ZnZrO_x$-400 had a more robust CO adsorption capacity, which was favorable for CO conversion. Therefore, the MOFs-derived oxides have abundant oxygen vacancies, and Zn-O-Zr localized structures, which are favorable for CO activation and the generation of methanol and dimethyl ether. Moreover, when combined with SAPO-34, the bifunctional catalyst containing MOFs-derived $ZnZrO_x$ achieved a CO conversion of 22.5% and a light olefin selectivity of 79.7% in hydrocarbons.

Due to the excellent CO dissociation and C-C coupling ability, Rh-based catalysts have shown excellent catalytic performance in ethanol synthesis via syngas conversion and have become popular catalysts for this catalytic system.[76] In order to compare the effects of pore size and junction properties of UiO MOFs on the catalytic performance of Rh-Mn catalysts, Mao et al. selected three UiO MOFs with different cavity sizes and SBUs and further prepared.[35] Rh-Mn bimetallic catalysts by impregnation method. Characterization results showed that the topology of the UiO MOFs was favorable for dispersing dense ultra-small Rh-Mn bimetallic nanoparticles. Among them, the Rh-Mn catalysts with Zr-UiO MOFs (UiO-66 and UiO-67) as supports exhibited outstanding catalytic performance, and the Rh/CeO_2 interface formed by the calcification of RM@Ce-UiO-66 facilitated the conversion of adsorbed CO to the stabilized carbonate species, which improved the activity.

Overall, compared with traditional materials, MOFs materials usually have higher specific surface area and tunable pore structure, which can help to improve the dispersion of catalytic active sites and the adsorption of reactant molecules during the Fischer-Tropsch reaction and thus increase the catalytic activity of FTS. On the other hand, through the precise design of MOFs structure and modification, the product distribution of FTS reaction can be modulated to a certain extent, for example, by adjusting the metal active center and functionalized ligands to improve the selectivity of specific hydrocarbon products. However, MOF materials often have the disadvantages of poor thermal stability

Table 2. Summary of the catalytic performance of MOFs and MOFs-derived catalysts for CO_2 hydrogenation to methanol reported in recent years

Entry	Catalyst	T (°C)	P (MPa)	GHSV[a] (mL g_{cat}^{-1} h^{-1})	H_2/CO_2	X_{CO} (%)	S_{MeOH} (%)	STY (g_{MeOH} $g_{cat}^{-1}h^{-1}$)	Reference
1	Cu/ZnO_x@UiO-66	250	4	12000	3	3.5	86.	1.27[b]	Yang et al., 2022[80]
2	CuO–ZnO@ZIF-8	200	2	2400	3	14.6	93.4	1.08	Zhanet al., 2023[82]
3	ZnO/Zr_{12}-bpdc	250	4	4800	3	7.5	95.0	0.11	Zhang et al., 2021[84]
4	15Cu/6.4ZnO/ AlFum MOF	230	5	10000	3	45.6	6.86	0.565	Duma et al., 2022[85]
5	3In@4Co(20)	300	5	15600	4	20.5	87.0	0.65	Pustovarenko et al., 2020[87]
6	12%Cu-ZrO_2-1-3	220	3	15000	3	6.8	64.4	0.288	Yu et al., 2021[88]
7	Cu-$ZnO^{MOF} \subset Al_2O_3$	240	3	14400	3	9.1	86.9	0.407	Qi et al., 2022[90]
8	Pd@In_2O_3	295	3	19200	3	8.0	81.0	81.1[c]	Cai et alk., 2022[91]
9	Cu@ZrO_2	220	3	15600	3	5.0	85.0	0.144	Han et al., 2022[92]
10	Mo-Co (2:1)-C-N (800)	275	2	6000	3	9.2	58.4	0.106	Hu et al., 2021[93]
11	h-MoS_2/ZnS	260	5	15000	4	9.0	67.3	0.93[days]	Zhou et alk., 2021[94]
12	CuZnO-MOF-74-350	190	4	4000	3	7.5	80.0	0.45	Zhou et al., 2023[95]
13	$Cu/ZnO_x/ZrO_2$	260	4	12000	3	18.7	52.0	0.217	Zhang et al., 2022[96]
14	Cu@ZrO_2-U	260	3	2400	3	12.1	70.5	0.073	Chen et al., 2023[100]
15	In–Co–Zn/C–N	300	2	6000	3	7.0	77.0	0.106	Liu et al., 2022[101]
16	In_2O_3@ZrO_2	290	3	12000	3	10.4	84.6	0.29	Cui et al., 2022[102]
17	Cr_2O_3/C-500-500	350	3	1200	3	16.8	29.9	0.038	Wang et al., 2023[105]

a g g_{Cu}^{-1} h^{-1}.
b g g_{Pd}^{-1} h^{-1}.
c g $g_{MoS2}^{-1}h^{-1}$.
[a]Gas hourly space velocity.

and high synthesis and processing costs, so MOFs-derived catalysts obtained by pyrolysis/carbonization are often used to obtain good stability, and there is still a need to optimize the synthesis and preparation strategies to improve their competitiveness in large-scale industrial applications.

CO_2 CONVERSION

Excessive CO_2 emissions from the combustion of fossil fuels have caused enormous environmental issues, such as global warming, ocean acidification, and climate change. Converting CO_2 into high-value-added chemicals is a promising strategy not only to reduce carbon emissions but also to fulfill the needs of sustainable development. Undoubtedly, MOFs have been widely used as a promising and powerful strategy for designing and producing a wide range of porous materials to address current environmental and energy issues worldwide. In the past few years, more and more MOFs have been used for CO_2 capture, regeneration, and conversion. In this section, we present recent research advances in using MOFs-based multiphase catalysts for the hydrogenation of CO_2 to valuable chemicals in three main routes: the methanol route, the modified Fischer-Tropsch route, and CO_2 methanation.

MOFs-based catalysts for CO_2 hydrogenation to CH_3OH

Among many valuable chemicals, methanol is not only a building block chemical but also a promising energy carrier for industry and vehicles. In some bifunctional catalytic systems, methanol can be a reaction intermediate for further conversion to other high-value chemicals. The catalytic activities of MOFs-based catalysts for CO_2 hydrogenation to methanol are summarized in Table 2.

To our knowledge, the first person to use MOFs for CO_2 hydrogenation to methanol was Yaghi. In 2016, Yaghi et al. reported a pioneering work in which they encapsulated 18 nm Cu nanocrystals (NC) into single crystal UiO-66 to obtain Cu $\subset$ UiO-66 for CO_2 hydrogenation to methanol.[77] The reaction was carried out at 175°C and 1 MPa, and the results showed that Cu/ZrO_2, Cu/UiO-66, Cu/ZnO/Al_2O_3, and Cu$\subset$UiO-66 displayed catalytic activity. Cu$\subset$UiO-66 possessed the highest methanol-forming transition frequency (TOF) of 3.7×10^{-3} s^{-1} and a 100% methanol selectivity. This work was the first to discover the strong metal-carrier interaction effect of MOFs-derived SBU, providing new insights into developing highly selective and efficient MOFs-based non-homogeneous catalysts. Assaf et al. recently synthesized xCu/MOFs catalysts for CO_2 hydrogenation to methanol by impregnating UiO-66 carriers with varying concentrations of copper precursors.[78] The Cu NP loading accounted for the missing linker defects in the UiO-66 structure, the highest copper-loaded 20Cu/MOFs catalysts had the highest CO_2 conversion and best methanol yields due to strong metal-support interactions and

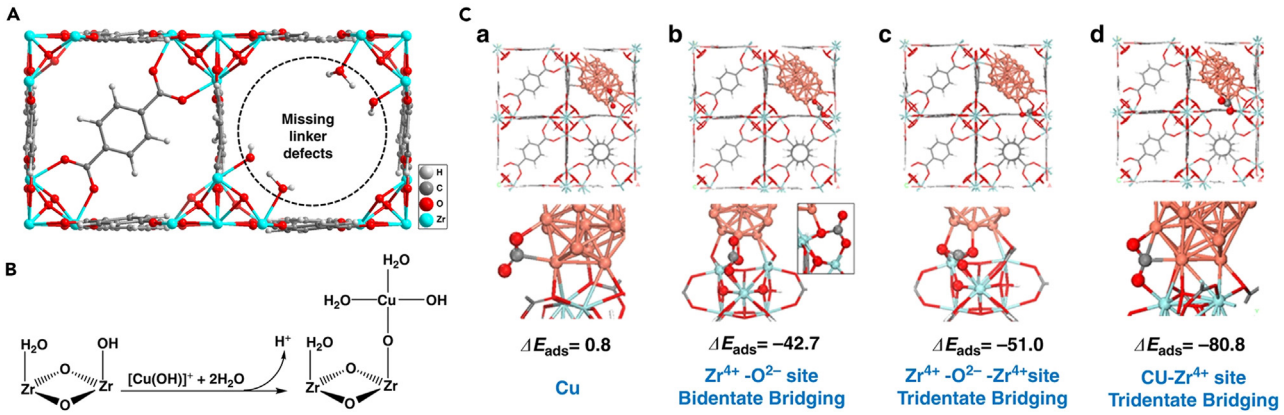

Figure 9. Using defective nodes to deposit Cu species

(A) A linker missing in the UiO-66 structure is replaced by two –OH/OH_2 species, which are active for ion exchange to deposit metal onto the Zr_6 nodes of the MOF.

(B) Possible reaction for Cu deposition (ion exchange) in aqueous solution.

(C) Adsorption energies (ΔE_{ads} in kJ/mol) of CO_2 at the Cu/UiO-66-a interface. a Cu only sites, b Zr^{4+}-O^{2-} sites on the Zr_6O_8 nodes in a bidentate bridging mode, c Zr^{4+}-O^{2-}- Zr^{4+} sites on the Zr_6O_8 nodes in a tridentate bridging mode, and d Cu-Zr^{4+} interfacial sites. Reproduced with permission from Zhu et al.[79] Copyright © 2020, Nature Publishing Group.

the highest number of missing linker defects in the MOFs structure. The breakthrough of this work enriches the understanding of the effect of copper loading on the UiO-66 and the influence of defect concentration on the catalytic performance. It contributes to the rational design of catalysts for CO_2 hydrogenation to methanol. Lercher and Gutiérrez prepared MOFs UiO-66 samples with controlled defect concentrations and confined Cu clusters in UiO-66 to obtain Cu/UiO-66 for use in the CO_2 hydrogenation to methanol.[79] They prepared Cu/UiO-66 by exchanging hydroxyl groups at the Zr_6O_8 node by hydrated hydroxyl Cu cations and finally obtained Cu/UiO-66-a with an optimal Cu loading of 1.4 wt %. At 250°C, 3.2 MPa (Figure 9), the methanol production rate of Cu/UiO-66-a was 4.7 mol$_{MeOH}$ mol$^{-1}_{Cu}$ h^{-1}, an order of magnitude higher than the rate using the reference Cu/ZrO_2. DFT and experimental desorption results indicate that the Zr-*O*-Cu interface is part of the active site that strongly adsorbs CO_2. This strategy supports the design of rational catalysts for CO_2 hydrogenation to methanol.

In recent years, the catalytic performance of Cu-loaded MOFs for CO_2 hydrogenation to methanol has been significantly improved by incorporating other metal additives such as Zn and has been widely used. Li et al. synthesized Cu/ZnO_x/UiO-66 for the first time using the dual-solvent method for CO_2 hydrogenation to methanol.[80] At 250°C, 4 MPa, for Cu/ZnO_x@UiO-66, the STY of methanol is enhanced by 5.5 and 8.5 times compared with those on the commercialized Cu/ZnO/Al_2O_3 and the Cu/ZnO @UiO-66 prepared with the traditional impregnation method. The double solvent method solves the problem that metal particles are easy to agglomerate, and Cu and ZnO phases can easily separate during the high-temperature reaction process. Thus, the prepared catalyst could show good stability. Kobayashi et al. prepared Cu-ZnO/amUiO-66 composites made of Cu-ZnO nanocomposites and amUiO-66 for CO_2 hydrogenation by spray-drying method (Figure 10A).[81] XRD, EXAFS, and STEM-EDX patterns showed that the Cu-ZnO nanocomplexes were homogeneously distributed in the UiO-66 material. In the CO_2 hydrogenation to methanol reaction, the catalytic activity of Cu/amUiO-66 was three times higher than that of crystalline UiO-66 (Figure 10B). In addition, the methanol yield of Cu-ZnO/amUiO-66 was increased by 1.5 times compared with that of Cu/amUiO-66. This study can help for the next step of MOF research. More recently, San et al. prepared a novel floral CuO-ZnO@ZIF-8 catalyst.[82] XPS and Raman spectra show that the CuO-ZnO@ZIF-8 surface has more oxygen vacancies than co-precipitated CuO-ZnO. XPS and Raman spectra analyses revealed that the CuO-ZnO@ZIF-8 surface exhibits higher oxygen vacancies (O_V) concentrations than co-precipitated CuO-ZnO. These oxygen vacancies play a crucial role in the hydrogenation reactions that lead to the formation of CH_3OH. The O_V sites facilitate the adsorption of H* species and CO_2, activating the reaction intermediates and reducing the energy barrier. Furthermore, the unique floral structural morphology of CuO-ZnO@ZIF-8 enhances the availability of O_V and exposed active sites, strengthening the coordination between CuO and ZnO, thereby favoring the conversion of CO_2 to CH_3OH. CuO-ZnO@ZIF-8 (1:4) demonstrates impressive performance, achieving 14.64% CO_2 conversion and 93.41% methanol selectivity at 200°C. This work further demonstrates that the combination of metals with MOFs can improve the efficiency of catalytic CO_2 hydrogenation to methanol.

In addition to Cu, other classical catalysts for CO_2 hydrogenation to methanol, such as Zn, Pt, etc., can also be combined with MOFs. Recently, Olsbye et al. investigated the kinetic role of Zr-nodes and the effect of H_2O on the CO_2 hydrogenation reaction on UiO-67-Pt at 170°C (Figure 11).[83] Through steady-state and transient isotope exchange experiments, H_2O co-feed measurements, and density-functional-theory (DFT) calculations, they discovered that an increase in the number of defects in the Zr-nodes accelerates the production rates of methanol and CH_4. Additionally, they observed that water promotes methanol desorption but does not alter the steady-state reaction rate of methanol formation. On the other hand, water has a significant inhibitory effect on CH_4 formation. These results suggest that water can be used to improve the selectivity of methanol and encourage further detailed investigation of the catalyst system.

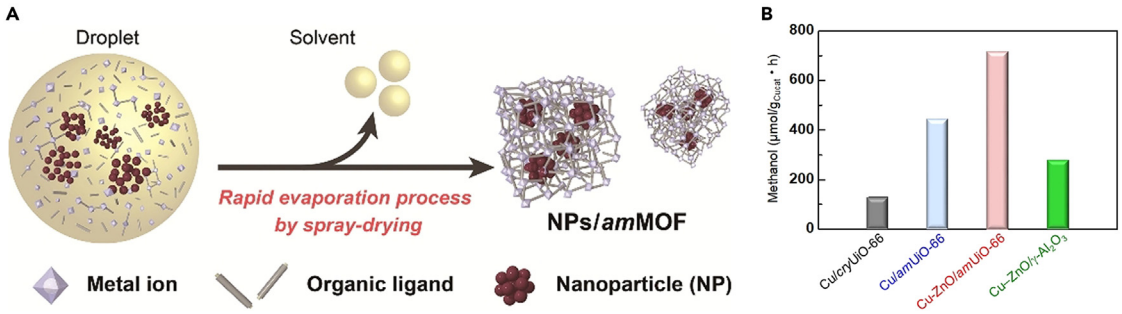

Figure 10. MOFs-based nanocomposites prepared by spray drying for CO_2 hydrogenation

(A) Cu/amUiO-66 and Cu-ZnO/amUiO-66 synthesized by the spray-drying method for highly enhanced catalytic activity of CO_2 hydrogenation for methanol synthesis.

(B) The amount of methanol synthesized from CO_2 and H_2 by Cu/cryUiO-66, Cu/amUiO-66, Cu-ZnO/γ-Al_2O_3, and Cu-ZnO/amUiO-66 catalysts. Reproduced with permission from Mitsuka et al.[81] Copyright © 2021, John Wiley and Sons.

Wang et al. loaded ZnO onto Zr-based MOFs to obtain ZnO/Zr_{12}-bpdc for the hydrogenation of CO_2 to methanol.[84] The Zr-based MOFs contained $Zr_{12}(\mu_3\text{-}OH)_8(\mu_3\text{-}OH)_8(\mu_2\text{-}OH)_6$ clusters, which were connected by linear biphenyl dicarboxylate (bpdc). The resulting ZnO/Zr_{12}-bpdc catalysts showed STY of up to 110 $mg_{MeOH}\ g_{cat}^{-1}\ h^{-1}$ or 440 $mg_{MeOH}\ g_{Zn}^{-1}\ h^{-1}$ and more than 95% selectivity for methanol at 250°C, 4 MPa. In this work, the ZnO/ZrO_2 interface was replaced by the contact between ZnO and Zr_{12} clusters in MOFs, providing insights into the chemical structure of the active sites in ZnO/ZrO_2 catalysts. Musyoka et al. used Cu-ZnO catalysts supported on an aluminum fumarate metal-organic framework (AlFum MOF) for CO2 hydrogenation to methanol.[85] The Cu and Zn active sites of the catalyst showed homogeneous dispersion. SEM, SEM-EDS, and TEM revealed that the morphology of the support is preserved after metal loading. The catalyst exhibited good activity with a doubling of Cu and Zn loading over AlFum MOF, leading to an increase in CO_2 conversion from 10.8% to 45.6% and methanol yield from 34.4 to 56.5 $g_{MeOH}\ kg_{cat}^{-1}h^{-1}$. The performance of catalysts loaded on AlFum MOF reveals that MOF has great promise for application in thermocatalytic conversion.

In addition to preparing catalyst support, MOFs can be used as a precursor for direct pyrolysis to prepare MOFs-based catalysts, which form porous carbon nanomaterials by heat treatment. In 2011, Xu et al. prepared nanoporous carbon materials with high specific surface area using zeolite-type MOFs as a precursor and templating agent and furfuryl alcohol as a second precursor.[86] Gascon et al. first applied this strategy to CO_2 hydrogenation to methanol.[87] They subjected indium-impregnated ZIF-67 to stepwise pyrolysis-oxidative decomposition to obtain In_2O_3@Co_3O_4 reticulated-shell composites with nanostructures. Under reaction conditions, the material underwent structural reorganization, transforming from Co_3O_4 with an amorphous In_2O_3 shell to layer-covered $Co_3InC_{0.75}$ consisting of a mixture of amorphous CoO_x and In_2O_3 oxides. Amorphous mixed cobalt-indium oxide shells lead to high yields and selectivity for methanol. The material can reach a maximum methanol production rate of 0.65 $g_{MeOH}\cdot g_{cat}^{-1}\cdot h^{-1}$.

Recently, Wu et al. prepared a series of ZrO_2@HKUST-1 composites, which were thermally decomposed to obtain Cu-ZrO_2 catalysts with highly dispersed Cu nanoclusters. These catalysts have high dispersion and large Cu-ZrO_2 interfacial area, which provided improved catalytic performance.[88] The results of experimental and DFT studies showed that the Cu-ZrO_2 interface not only activated CO_2 but also stabilized the intermediates, indicating that the interface plays a crucial role in the conversion of CO_2 and the selective generation of methanol. Jin et al. prepared highly dispersed copper/graphene catalysts using HKUST-1 as a template agent.[89] The graphene/Cu/Zn catalysts were first prepared and calcined at 800°C in nitrogen to obtain GCZ4-800 catalysts. Calcination resulted in uniform dispersion of Cu active centers on graphene. The synergistic effect of graphene and HKUST-1 enhanced the specific surface area of the catalyst, the reducibility of the Cu active centers, and the adsorption capacity for H_2 and CO_2. Compared with the traditional impregnation method, this strategy solved the problems of uneven distribution of active centers and low loading. It provided a new method to achieve the control of metals on carriers.

The MOFs direct pyrolysis strategy cannot only enable nanoparticles to inherit precursor morphology but also integrate multiple functionalities. Bimetallic MOF templates offer unique advantages, such as interfacing with catalytically active metals and enhancing synergetic effects and stability through "solid solution" or "core-shell" structures. Song et al. synthesized bimetallic CuZn-BTC catalysts by a modified one-pot solvothermal method.[90] The Cu-ZnO^{MOF}/Al_2O_3 catalysts achieved 86.9% methanol selectivity and 407.2 $g_{MeOH}^{-1}kg_{cat}^{-1}h^{-1}$ methanol STY at 240°C and 3.0 MPa. Characterization by TEM, XPS, EDX, *in-situ* DRIFTS, chemisorption and programmed warming desorption showed that the novel Cu-ZnO^{MOF}/Al_2O_3 catalysts have high Cu dispersion on the surface, surface-enriched ZnO and a high number of Cu-ZnO interfacial sites, which improve the adsorption and activation capacity of the catalysts for CO_2 and H_2. This work provides new ideas for optimizing the activity and selectivity of amorphous Cu/ZnO/Al_2O_3 catalysts in CO_2 hydrogenation to methanol reaction. Li et al. synthesized Pd@In_2O_3 catalysts using TCPP(Pd)@MIL-68(In) as a sacrificial templating agent to enhance the dispersion of Pd^0 species over In_2O_3 and to prevent the formation of the In-Pd super reduced phase (Figure 12A).[91] Under the conditions of 295°C and 3 MPa, the Pd/In_2O_3 catalyst exhibited a maximum methanol STY of 81.1 $g_{MeOH}\ g_{Pd}^{-1}\ h^{-1}$, with CO_2 conversion of 8.0%, and 81% methanol selectivity (Figure 12B). The experimental results indicate that the degree of reduction of In_2O_3 can be controlled by regulating the electronic interactions between Pd and In_2O_3 to improve the methanol selectivity. This study provides a method for designing highly active methanol synthesis catalysts.

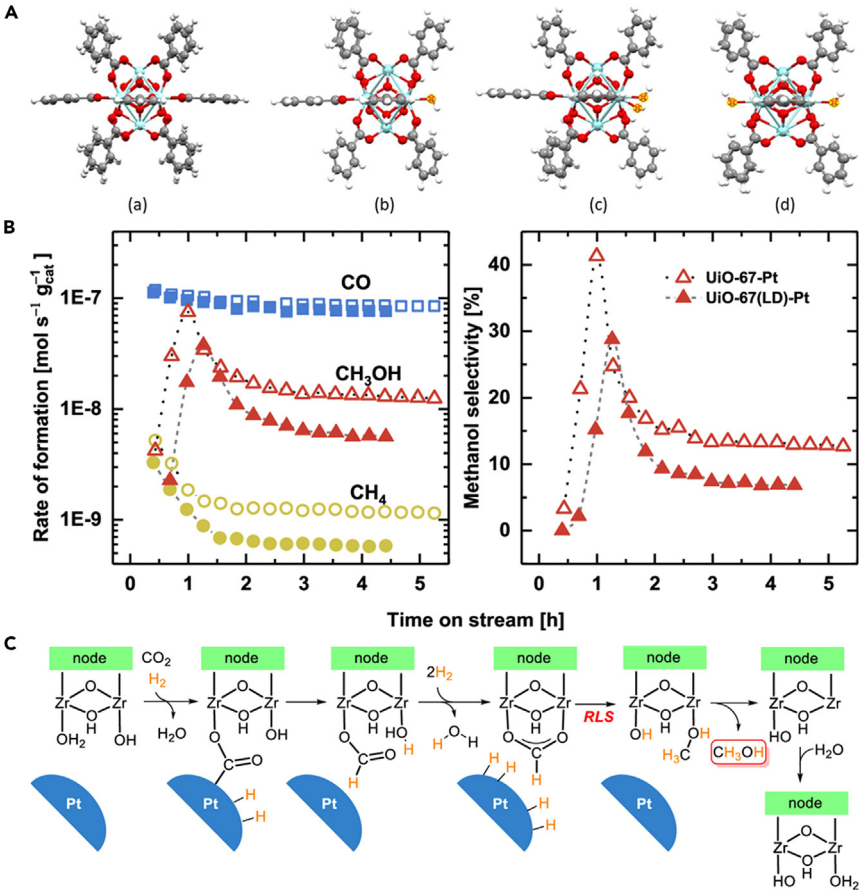

Figure 11. The kinetic role of Zr-nodes and the effect of H_2O on the CO_2 hydrogenation reaction

(A) a Zirconium node with 12 benzoate linkers. b A defective node is created by removing one linker resulting in a Zr-node with 11 linkers. c A defective node with two adjacent missing linkers. d A defective node with two opposite missing linkers. The carbon atoms furthest away from the Zr-node were constrained in all cases in all directions, to simulate the integrity of the UiO-67 MOF.

(B) Reaction-onset comparison of UiO-67-Pt (open symbols) and UiO-67(LD)-Pt having intrinsically less benzoic acid modulator (filled symbols). Left: CO (squares), CH_3OH (triangles), and CH_4 (circles) rate of formation. Right: methanol selectivity versus time on stream. Conditions: CO_2/H_2/inert = 1/3/1, τ = 0.01 g_{cat} min ml^{-1}, T = 170°C, 8 bar.

(C) Postulated mechanism for methane formation on an open Zr-site at the UiO-67-Pt Zr-node. Reproduced with permission from Gutterød et al.[83] Copyright © 2020, American Chemical Society.

MOFs pyrolysis can also be used to form unique catalyst structures. Ma et al. prepared hollow Cu@ZrO_2 catalysts for CO_2 hydrogenation to methanol by pyrolyzing Cu-loaded Zr-MOFs.[92] Firstly, MOF808 precursor was prepared, and Cu was loaded on the precursor and then calcined at different temperatures. CM-300 obtained by calcination at 300°C was the best catalyst for CO_2 hydrogenation to methanol, with a CO_2 conversion of 5% and methanol selectivity of 85% at 220°C. The Cu nanoparticles generated by low-temperature pyrolysis had highly dispersed Cu^0/Cu^+ equilibrium sites, a large number of surface basic sites, and abundant Cu-ZrO_2 interfaces, which contributed to the enhancement of the catalyst's CO_2 adsorption/activation and selective hydrogenation to methanol.

Mo-based catalyst is an efficient catalyst for CO_2 hydrogenation to methanol.[93–95] Li et al. synthesized Mo-Co-C-N catalysts using ZIF-67 as a precursor for CO_2 conversion to methanol.[96] The highest methanol STY was achieved by Mo-Co (2:1)-C-N (800) catalysts at 275°C and 2 MPa,. The formation of Mo_2C and $Co_6Mo_6C_2$, formed during catalyst preparation, can be used as active phases for RWGS and methanol synthesis reactions. The experimental results showed that the formation of more oxygen vacancies at higher roasting temperature (800°C) can promote CO_2 desorption and improve methanol selectivity. In-plane sulfur vacancies in MoS_2 nanosheets have been identified as efficient catalytic active sites for methanol synthesis from CO_2, while edge vacancies facilitate CO_2 to methane. Zeng et al. prepared boxlike assemblages of quasi-monolayer MoS_2 nanosheets (h-MoS_2/ZnS) by a solvothermal route of MOFs bonding and subsequent thermal treatment (Figure 13).[97] With the increased exposure of in-plane sulfur vacancies and decreased occurrence of edge sulfur vacancies, h-MoS_2/ZnS exhibited impressive performance, achieving methanol selectivity of 67.3% and CO_2 conversion of 9.0%, with methanol STY as high as 0.93 g_{MeOH} g_{MoS2}^{-1} h^{-1} at 260°C, 5 MPa. The presence of ZnS can effectively prevent reacting molecules from accessing the sulfur vacancies at the edges of MoS_2 nanosheets, thus improving the selectivity of the

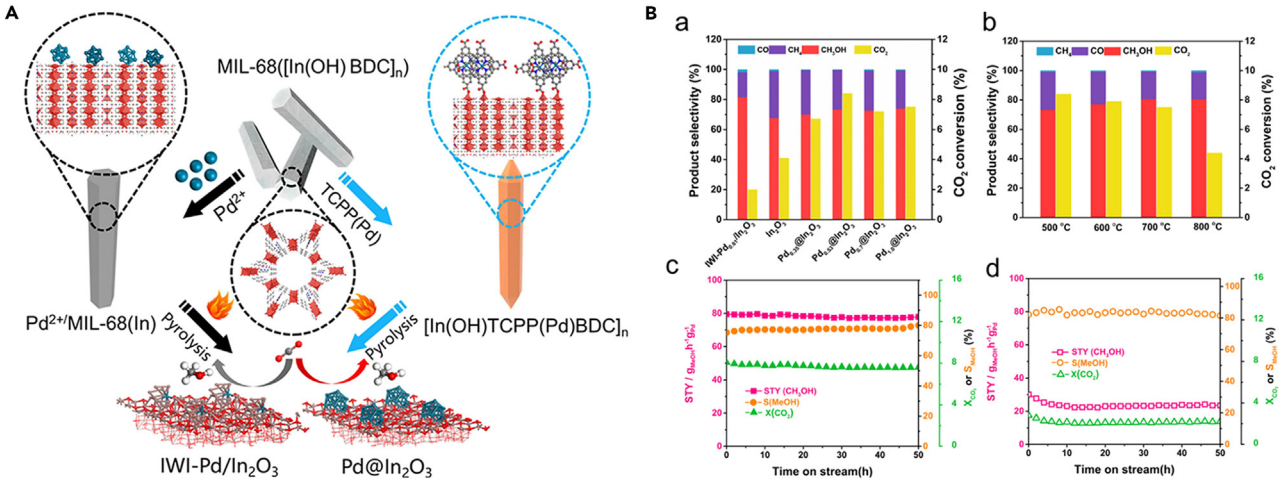

Figure 12. Using MOFs sacrificial templating agent to enhance the dispersion of Pd^0 species over In_2O_3

(A) Fabrication Routes of Pd^{2+}/MIL-68(In) and TCPP(Pd)@MIL-68(In) Composites and the Derived IWI-Pd/In_2O_3 and Pd@In_2O_3 Catalysts (B) a Catalytic performance of various Pd-In_2O_3 catalysts, b catalytic performance of Pd@ In_2O_3 catalysts prepared under varied calcination temperatures, c time of stream of Pd@ In_2O_3-600, and d IWI-Pd/In_2O_3 catalyst under standard reaction conditions. Reproduced with permission from Cai et al.[91] Copyright © 2022, American Chemical Society.

target product methanol. This study not only provides a MOFs-involved route for the preparation of hollow quasi-monolayer MoS_2 nanocartridge catalysts but also develops a new method to block or generate the edge sulfur vacancies, which offers fresh perspectives on enhancing CO_2 hydrogenation to methanol conversions.

The Cu-ZnO interface concentration is an essential factor in the hydrogenation of CO_2 to methanol catalyzed by the Cu/ZnO catalyst. Li et al. prepared a Cu/ZnO catalyst (CuxZnO-MOF-74-350) with a Cu-rich-ZnO interface using the Cu-Zn bimetallic MOFs template method (x is the Cu/Zn feed ratio).[98] At 210°C, 4 MPa, when the feeding Cu/Zn ratio was optimized as 1:1, the catalyst exhibited a CO_2 conversion of 6.3% and a methanol STY of 0.29 $g \cdot g_{cat}^{-1} \cdot h^{-1}$. Combined with TEM, HRTEM, chemisorption, and EPR, it was concluded that a suitable Cu/Zn ratio is favorable to improve the adsorption and activation of H_2 and CO_2, and the ordering of Cu and Zn, which results in a rich Cu-ZnO interface and promotes the formation of methanol. Similarly, Li et al. prepared a highly efficient and stable CO_2 hydrogenation to methanol catalyst (Cu/ZnO_x/ZrO_2) by co-precipitation and pyrolysis using UiO-66 as a template agent.[99] The STY of methanol on the Cu/ZnO_x/ZrO_2 catalysts

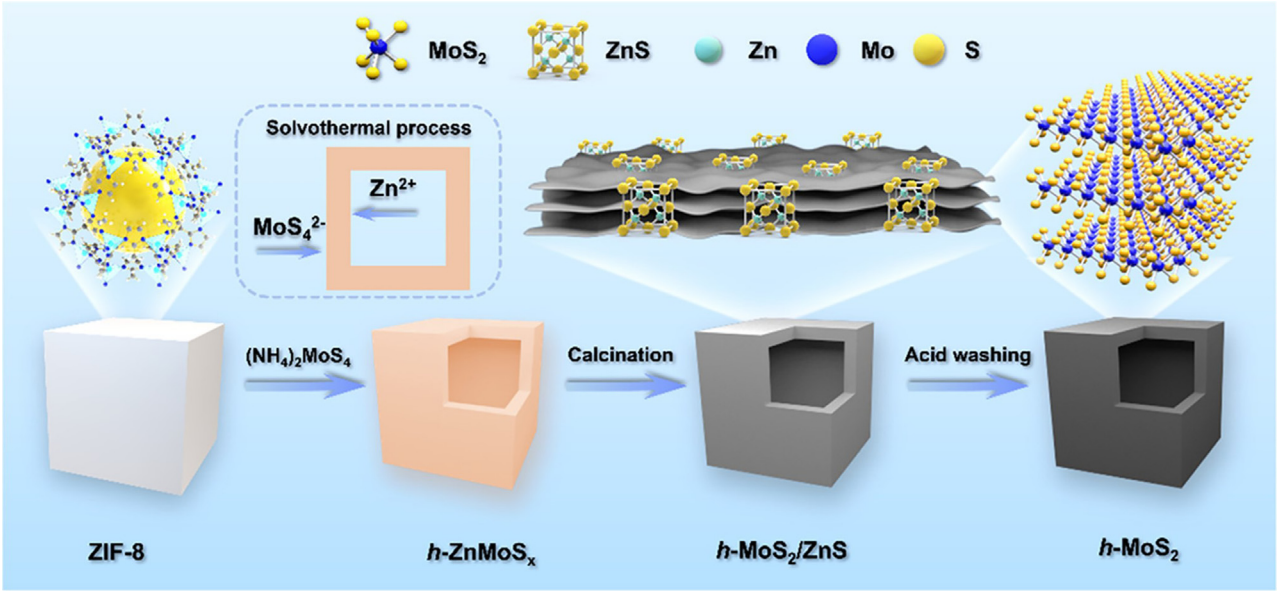

Figure 13. Schematic illustration of the hollowing synthetic route: formations of h-$ZnMoS_x$, h-MoS_2/ZnS, and h-MoS_2, starting from their precursor ZIF-8 nanocubes

Reproduced with permission from Zhou et al.[97] Copyright © 2022, American Chemical Society.

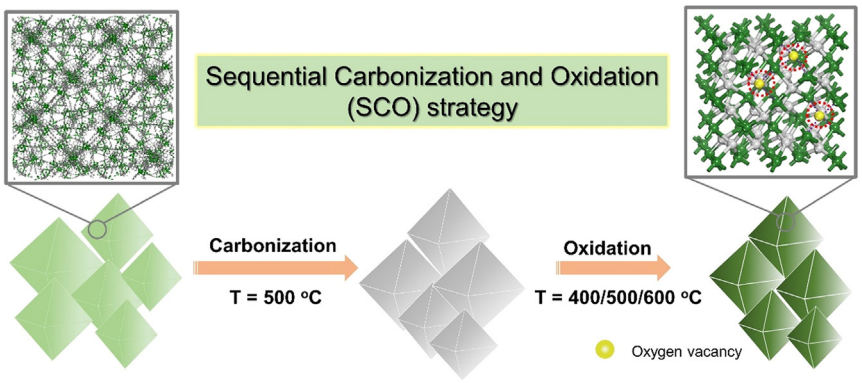

Figure 14. Fabrication procedure of SCO-derived Cr_2O_3 catalyst
Reproduced with permission from Wang et al.[105] Copyright © 2023, John Wiley and Sons.

was as high as 216.7 g_{MeOH} kg_{cat}^{-1} h^{-1} at 260°C and 4 MPa. The UiO-66-derived ZrO_2 carrier enhanced the interaction between the carrier and Cu/Zn, significantly improving the catalytic performance. In this study, the catalytic effect was enhanced by pyrolysis to decompose the MOFs material to expose more active sites.

The loading of active components in MOFs-based catalysts can be controlled simply by the deposition-precipitation method. Mao et al. prepared a series of Cu@UiO-67 catalysts with different Cu loadings by deposition-precipitation method using, and then the Cu@ZrO_2-U obtained by pyrolysis Cu@UiO-67 was used forCO_2 hydrogenation to methanol.[100] Among them, 20-Cu@ZrO_2-U catalysts exhibited the best catalytic activity at 3 MPa and 260°C, and the STY of CH_3OH reached 2.28 $mmol_{CH3OH}$ g_{cat}^{-1} h^{-1}. The three-dimensional skeleton with UiO-67 in the Cu@ZrO_2-U catalyst immobilized highly dispersed copper nanoparticles, and the CuO_2-ZrO_2 interface was obtained by controlling the copper content, which enhanced the synergistic effect of copper and ZrO_2-U, thus significantly improving the catalytic activity. The *in situ* DRIFTS results indicate that the methanol synthesis via CO_2 hydrogenation on 20-Cu@ZrO_2-U follows the HCOO* intermediate reaction pathway.

In_2O_3-based catalysts hold promise in CO_2 hydrogenation to methanol with high selectivity, yet low conversion hinders their practical use. He et al. report an In-Co-Zn/C-N catalytic system for hydrogenating CO_2 to methanol.[101] The In-Co-Zn/C-N-4 (PM) has high conversion and stability and was found to keep a stable STY of 3.3 mmol g_{cat}^{-1} h^{-1} for methanol over a 50 h period at 2 MPa and 300°C. Since cobalt-indium carbide inhibits methanol production, ZnO weakens the interaction between Co and In to some extent and inhibits the formation of $Co_3InC_{0.75}$, which enhances the selectivity of methanol. Due to its high activity, the In_2O_3/ZrO_2 catalyst is widely used in methanol synthesis, yet the electronic interactions at its interface remain elusive. Hu et al. obtained In_2O_3@ZrO_2 with a hollow structure and abundant In_2O_3/ZrO_2 heterointerfaces by pyrolysis of the mixed MOFs precursor MIL-68@UiO-66.[102] The In_2O_3@ZrO_2 catalyst exhibited an activity of 0.29 g_{MeOH} g_{cat}^{-1} h^{-1} at 290°C and 3.0 MPa. Mechanistic studies have shown that the electrons at the In_2O_3@ZrO_2 heterogeneous interface tend to be transferred from ZrO_2 to In_2O_3 due to strong interactions to generate electron-rich In_2O_3, which promotes the conversion of HCOO∼* to CH_3O∼* in the process of methanol synthesis. This work reveals the key role of heterointerfaces in regulating the activity and selectivity of CO_2 hydrogenation to methanol.

Methanol can also serve as a reaction intermediate to generate other high-value chemicals. In recent years, many studies have combined MOFs-based catalysts with molecular sieves to modulate the product distribution of CO_2 hydrogenation. Zhang et al. prepared $ZnZrO_x$/SAPO-34@UiO-n (n = 66, 66-NH_2, and 67) tandem catalysts for the catalytic conversion of CO_2 to light olefins.[103] They coated UiO-n shells on monodisperse SAPO-34 zeolites and physically mixed them with $ZnZrO_x$ by grinding to obtain $ZnZrO_x$/SAPO-34@UiO-n catalysts. $ZnZrO_x$/SAPO-34@UIO-66 showed the highest light olefin selectivity (80%) at 380°C, 3 MPa, and it was found that the type of UiO-n membrane could influence the CO_2 hydrogenation product distribution. Dusselier et al. obtained an In-Zr/zeolite hybrid catalyst by directly calcinating MOFs ((Zr)Ui0-67-bipy-In) in the presence of zeolites.[104] The excellent dispersion and low loading of MOFs-derived In-Zr oxides complemented by the strong acidity of rhodochrosite-type zeolites allowed the combination of the activation of CO_2 with the C-C coupling at the employed GHSV conditions to have high STY of light olefins at 375°C. This work reports for the first time the use of small-pore zeolites as acid catalysts instead of zeolite types, demonstrating the importance of acid strength and acidity control by varying the Si/Al ratio for catalyzing CO_2-methanol-olefin cascades.

More recently, Wu et al. obtained Cr_2O_3 catalysts with high oxygen vacancy (O_v) density by sequential carbonization and oxidation (SCO) of chromium-based MOFs (Figure 14).[105] The methanol selectivity of the Cr_2O_3/C-500-500 catalyst was as high as 98.1% at 350°C, 3 MPa with 16.8% CO_2 conversion due to O_v enrichment. Subsequently, they combined the Cr_2O_3/C catalyst with acidic H-ZSM-5 to realize the direct conversion of CO_2 to aromatics. This work provides a synergistic strategy for improving the performance of CO_2 hydrotreating to aromatics by the cooperation of plenty of O_v in reducible metal oxide, unique accessibility of reactants to O_v active sites, and ingenious Al location in zeolite channels. Later, Wu et al. further combined the above Cr_2O_3/C with Cu-doped H-ZSM-5^T to convert CO_2 directly to paraxylene (PX).[106] The PX selectivity and STY achieved 33.8% and 3.0 g_{CH2} kg_{cat}^{-1} h^{-1}, respectively, by the bifunctional catalysts Cr_2O_3/C & Cu-ZSM-5^T@SiO_2. This study provides a bifunctional catalyst design strategy for CO_2 hydrogenation into targeted products.

Table 3. Summary of the catalytic performance of MOFs and MOFs-derived catalysts for CO_2 hydrogenation by modified Fischer-Tropsch route reported in recent years

Entry	Catalyst	T (°C)	P (MPa)	GHSV (mL g_{cat}^{-1} h^{-1})	H_2/CO	X_{CO2} (%)	S_{CO} (%)	S_{CH4} (%)	Desired product (%)	Reference
1	Na-Fe@C& H-ZSM-5-0.2 M	320	3	9000	3	15.5	55.5	49	8.2 of aromatics	Wang et al., 2020[108]
2	Na-Fe@C/ H-ZSM-5-0.2 M	320	3	9000	3	13.3	13.3	4.8	50.2 of aromatics	Wang et al., 2020[108]
3	Na-Fe@C|| H-ZSM-5-0.2M	320	3	9000	3	29.5	15	7.3	46.1 of aromatics	Wang et al., 2020[108]
4	2%Na-Fe@C/ CuZnAl	320	5	4500	3	37.1	9.2	3.5	28.6 of ethanol	Wang et al., 2021[109]
5	2%Na-Fe@C/ 5%K-CuZnAl	320	5	4500	3	39.2	9.4	4.7	35.0 of ethanol	Wang et al., 2021[109]
6	MnFe/C	400	2	12000	3	37.6	28.3	16.78	57.9 of C_{5+}	Yang et al., 2023[110]
7	ZnFe/C	400	2	12000	3	40.6	22.9	26.68	40.5 of C_{5+}	Yang et al., 2023[110]
8	NiFe/C	400	2	12000	3	45.9	12.0	52.36	30.8 of C_{5+}	Yang et al., 2023[110]
9	Fe/C	400	2	12000	3	46.1	15.8	15.12	59.6 of C_{5+}	Yang et al., 2023[110]
10	Na-Fe@C-3D-sta	320	3	9000	3	32.1	17.2	23.5	48.5 of $C_2^{=}$~$C_4^{=}$	ang et al., 2024[111]
11	Na-Fe@C-3D-str	320	3	9000	3	39	15.9	23.8	48.9 of $C_2^{=}$~$C_4^{=}$	Wang et al., 2024[111]
12	Na-Fe@C-3D-spi	320	3	9000	3	38.5	16.6	23.7	50.7 of $C_2^{=}$~$C_4^{=}$	Wang et al., 2024[111]
13	Na-Fe@C	320	5	9000	3	25.5	22.2	17.3	12.0 of ethanol	Wang et al., 2023[112]
14	Na-ZnFe@C	320	5	9000	3	38.4	7.6	15	20.3 of ethanol	Wang et al., 2023[112]
15	Na-CuFe@C	320	5	9000	3	33.9	6.1	11.1	15.0 of ethanol	Wang et al., 2023[112]
16	Na-MnFe@C	320	5	9000	3	33.1	10.6	14.9	13.4 of ethanol	Wang et al., 2023[112]
17	Na-CoFe@C	320	5	9000	3	30.4	11.3	14.4	12.0 of ethanol	Wang et al., 2023[112]

MOFs-based catalysts for modified-FTS of CO_2 conversion

In addition to the methanol intermediates, the modified Fischer-Tropsch route (RWGS+FTS) is another CO_2 hydrogenation route in which CO_2 is first reduced to CO by the reverse water gas shift (RWGS) reaction. Then, CO is converted by the Fischer-Tropsch synthesis (FTS) reaction. In recent years, breakthroughs have been made in producing high-value chemicals by the modified Fischer-Tropsch route. The catalytic activities of MOFs-based catalysts for CO_2 hydrogenation via the modified Fischer-Tropsch route are summarized in Table 3.

In 2015, Makkee and Gascon et al. used MOFs-derived Fe-based catalysts for the first time to produce high-value chemicals via the FTS route.[36] Subsequently, in 2018, Gascon et al. prepared a highly active, selective, and stable Fe-based catalyst by pyrolysis of MOFs doped with different metal promoters to investigate its CO_2 hydrogenation performance.[107] The promoter-added catalyst achieved a high STY of C_2-C_4 olefins of 33.6 mmol g_{cat}^{-1} h^{-1} and CO_2 conversion of 40%, at 320°C and 3 MPa. The results showed that only K could significantly improve the selectivity of olefins in the reaction products among the different metal promoters.

Recently, Tsubaki et al. prepared Na-modified Fe-based catalysts by pyrolysis of Fe-MOFs and combined them with hollow acidic zeolite H-ZSM-5 to obtain bifunctional catalysts for one-pass conversion of CO_2 hydrotreating to aromatics (Figure 15).[108] The Fe-based catalyst portion of the bifunctional catalyst has abundant high-activity sites and special catalytic interfaces, which is conducive to the enhancement of CO_2 activation efficiency and the formation of olefin intermediates. The generated olefins diffuse into the acidic sites of H-ZSM-5 and are converted into aromatics via a dehydroaromatization reaction. The synergistic effect of the modified Fe-based catalysts and molecular sieves in this strategy significantly improved the selectivity of aromatics synthesis in CO_2 conversion. The carbon layers enhance the dispersion of Fe-based nanoparticles derived from MOFs, preventing aggregation during the catalytic process. It provided experience in catalyst design for the preparation of high-value-added products by CO_2 hydrogenation.

Later, Wang et al. obtained a novel multifunctional catalyst for CO_2 hydrogenation by combining Na-Fe@C with K-doped CuZnAl. (Figure 16).[109] They realized the direct conversion of CO_2 to ethanol and, simultaneously, could generate high-value olefins. The experimental results showed that the unique catalytic interface, close synergy, and aldehyde intermediates of the multifunctional catalyst played essential roles in the efficient conversion of CO_2 to ethanol. In addition, the catalyst has considerable potential for industrial applications due to its advantages of easy preparation, low cost, and easy recycling.

In order to study the effect of metal additives on the physicochemical properties and catalytic performance of Fe-based catalyst during CO_2 hydrogenation, Yu et al. prepared a series of transition metal M (M = Zn, Ni, Mn) modified Fe-based catalysts (MFe/C) by pyrolysis of MOFs for CO_2 hydrogenation.[110] The Mn-doped Fe-based catalysts exhibited optimal catalytic performance with 37.60% CO_2 conversion

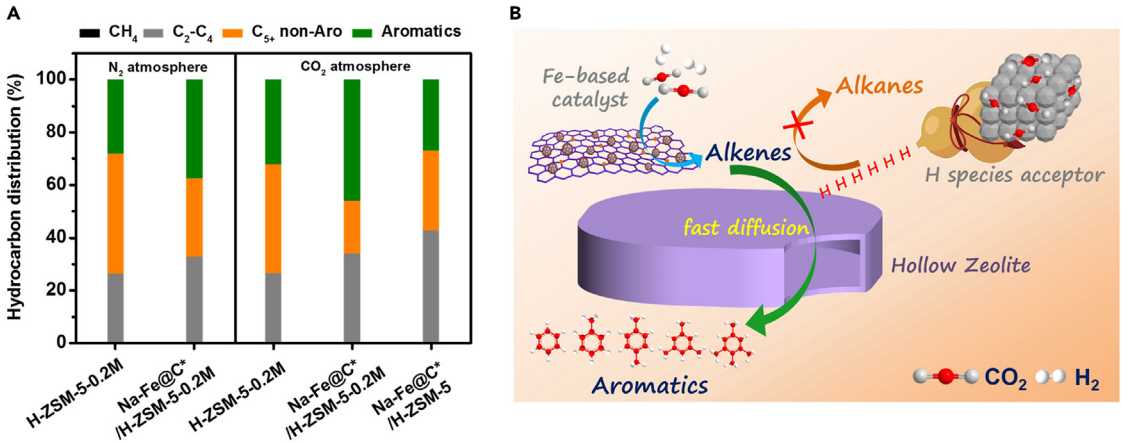

Figure 15. Combining Fe-based catalyst obtained from MOFs pyrolysis and acidic zeolite H-ZSM-5 for CO_2 hydrogenation to aromatics

(A) Catalytic performances of 1-hexene conversion over H-ZSM-5-0.2 M, Na-Fe@C*/H-ZSM-5-0.2 M (Na-Fe@C* represents the used Na-Fe@C), and Na-Fe@C*/H-ZSM-5 under N_2 or CO_2 atmosphere. Reaction conditions, 320 °C, 2 MPa, catalyst weight 1 g zeolite and 0.33 g Na-Fe@C*, liquid 1-hexene flow rate 0.005 mL min−1, TOS = 8 h.

(B) Schematic representation of the cooperative interplay between the multifunctional catalyst for the enhanced aromatics synthesis from CO_2 hydrogenation. Reproduced with permission from Wang et al.[108] Copyright © 2020, Elsevier.

and C_{5+} STY of 0.27 mol g_{cat}^{-1} h^{-1} under the reaction conditions of 400°C, 2.0 MPa. The metal additives Zn and Mn were able to promote the formation of the Fe_5C_2 active phase on the Fe-based catalysts, with the difference that Mn inhibited the secondary hydrogenation of olefins, while Zn enhanced the secondary hydrogenation of olefins. In addition, the content of specific Fe sites in Fe_5C_2 was found to be related to O/P and olefin selectivity. This study provides new ideas for designing catalysts with high catalytic performance regarding the effects of different metal additives on the active sites of Fe-based catalysts.

In practical reactions, catalysts often need to be formulated into pellets or monoliths for optimal mass and heat transfer. However, existing MOFs-based catalysts are often carbonaceous powders, making it challenging to shape them into suitable forms. Wang et al. fabricated Fe-based monolithic catalysts with excellent catalytic properties and specific structures by direct ink writing (DIW)-style 3D printing (Figure 17).[111] The helically structured Fe-based monolithic catalysts exhibited 52.6% light olefin selectivity and 451.8 g_{CH2} kg_{cat}^{-1} h^{-1} STY at 320°C, 3 MPa. The mass transfer simulation results indicate that the helically structured channels in the Fe-based monolithic catalysts are able to optimize the mass transfer by reducing the coverage of intermediates and products at the catalytic interfaces. This results in efficient utilization of the active centers and timely termination of the carbon chain growth. Density Functional Theory (DFT) showed that the relatively electron-rich catalytic interface and lower intermediate coverage could promote olefin desorption and inhibit the further growth of carbon chains, thus

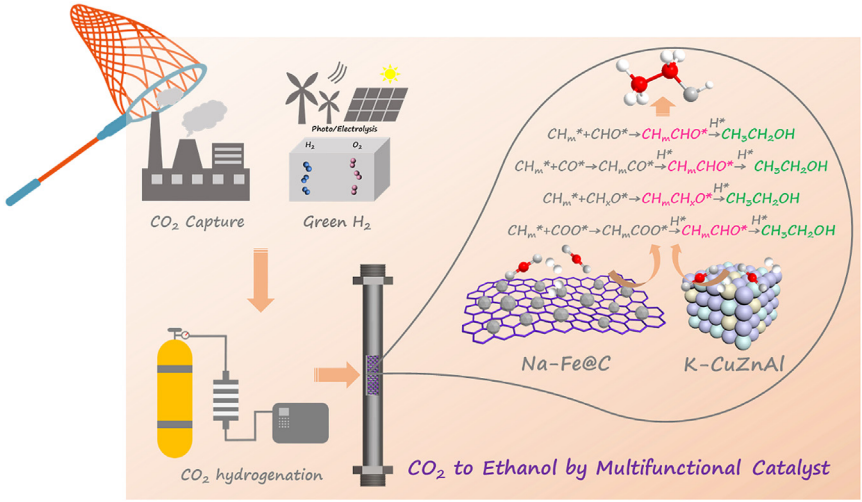

Figure 16. Schematic diagram of the direct conversion of CO_2 to ethanol

Reproduced with permission from Wang et al.[109] Copyright © 2021, American Chemical Society.

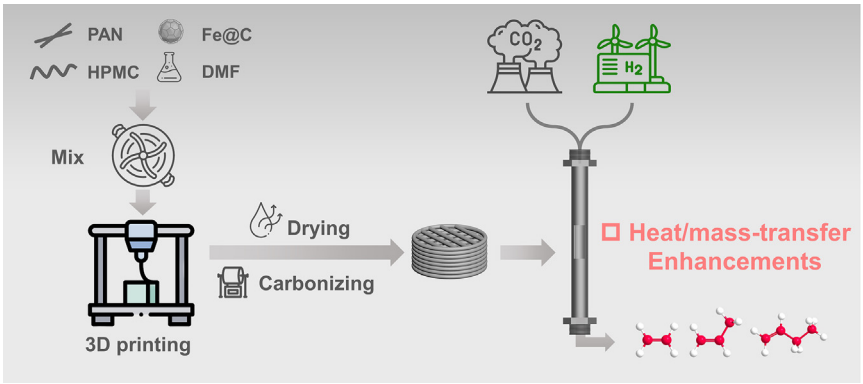

Figure 17. Schematic illustration for the fabrication of Fe-based monolithic catalysts via 3D printing technology
Reproduced with permission from Wang et al.[111] Copyright © 2023, Elsevier.

synergistically enhancing the synthesis performance of low-carbon olefins. As a result, the structure enhances the mass and heat transfer and avoids active site aggregation and carbon deposition, significantly improving the catalytic performance. This strategy also provides a new concept for modulating the CO_2 hydrogenation performance of Fe-based catalysts, and it can be generalized to the rational design of other catalytic materials.

The electronic properties of a catalyst play a crucial role in determining the adsorption strength and configuration of key intermediates, thereby influencing the reaction network for targeted synthesis. Wang et al. balanced the electronic properties of Fe species by adding a carbon buffer layer on the ternary catalytic component ZnO_x-Fe_5C_2-Fe_3O_4 (Figure 18).[112] This layer neutralizes excessive electrons transferred from ZnO_x to Fe species. The unique electronic properties, characterized by appropriate CO adsorption strength and C-C coupling barrier, facilitate ethanol synthesis via the -CO* insertion mechanism. This mechanism differs from the common ZnO_x-Fe_5C_2-Fe_3O_4 catalyst, which primarily produces alkenes or alkanes. The moderate CO adsorption strength on Fe_3O_4 and Fe_5C_2 and the low C-C coupling capacity between -CH_2* and -CO* on Fe_5C_2 synergistically resulted in an ultra-high ethanol STY of up to 366.6 $g_{EtOH}\ kg_{cat}^{-1}h^{-1}$ for CO_2 hydrogenation with a total addition of 10 Vol % CO. This study's carbon-based electron buffering strategy provides new ideas for the design of other electronic property-sensitive catalytic materials to achieve efficient catalytic performance.

MOFs-based catalysts for CO_2 hydrogenation to CH_4

CO_2 methanation, also known as the Sabatier reaction, was initially discovered by Paul Sabatier in 1902 and has since been extensively researched. This process is highly exothermic and thermodynamically favorable. Thermodynamically, the reaction is limited by thermodynamic equilibrium at high temperatures, and low temperature is conducive to positive reaction. Kinetically, however, the reaction rate of CO_2 methanation is relatively slow at lower temperatures, prolonging the production cycle. Consequently, the quest for novel and highly active catalysts is crucial to enhancing the yield of this reaction. Historically, metals such as Ni, Co, Ru, and Rh, supported on diverse supports., have demonstrated remarkable activity in CO_2 methanation.[113,114] Recently, MOFs have emerged as auspicious porous materials for CO_2 methanation reactions. Their unique properties offer countless possibilities for further enhancement and development, holding great promise for maximizing the production of renewable CH_4.

As far as we know, the initial investigation of the application of MOFs in CO_2 methanation was reported by Zhen et al. in 2015.[115] In their study, a series of highly active catalysts xNi@MOF-5 for CO_2 methanation were prepared by impregnation methods. Notably, the 10Ni@MOF-5 catalyst demonstrated unexpectedly superior activity compared to the reference catalyst Ni/SiO_2 at low temperatures ranging from 180°C to 320°C. Comprehensive characterization studies revealed that the uniform dispersion of Ni within the MOF-5 framework is the key factor underlying this remarkable activity enhancement. Furthermore, the 10Ni@MOF-5 catalyst demonstrated remarkable stability, exhibiting minimal deactivation during long-term stability tests lasting up to 100 h. These findings highlight MOF-5 as a promising and innovative support material for preparing CO_2 methanation catalysts.

Ni/CeO_2 is a highly active catalyst for CO_2 methanation, but its performance often suffers from nanocrystal coarsening at high temperatures.[116] To overcome this, Feng et al. designed a novel Ni/CeO_2 catalyst using Ce-based MOFs as a template (Figure 19).[117] This approach confinement effect of the MOF's ultra-small pores led to ultrafine Ni nanoparticles, excellent dispersion, and robust thermostability. Among the samples, the catalyst calcined at 600°C emerged as the most effective due to its abundant oxygen vacancies, which helped improve the CO_2 adsorption ability and the catalytic performance toward CO_2 methanation. This study presents a concise method for synthesizing ultrafine metal/metal oxide nanocomposite catalysts with superior catalytic activity and stability for diverse applications.

Carbon capture and conversion are often separate processes, with sorbents handling CO_2 enrichment and catalysts facilitating its transformation. Zurrer et al. introduced NiMg-CUK-1, a dual-functional MOFs, that seamlessly integrates both tasks.[118] By regulating the thermal stability of its Ni and Mg components, Ni nanoparticles are selectively formed within the Mg-rich framework. Optimization of the Ni: Mg ratio and treatment temperature boosts catalytic performance while maintaining CO_2 capture abilities. NiMg-CUK-1 efficiently captures CO_2 at

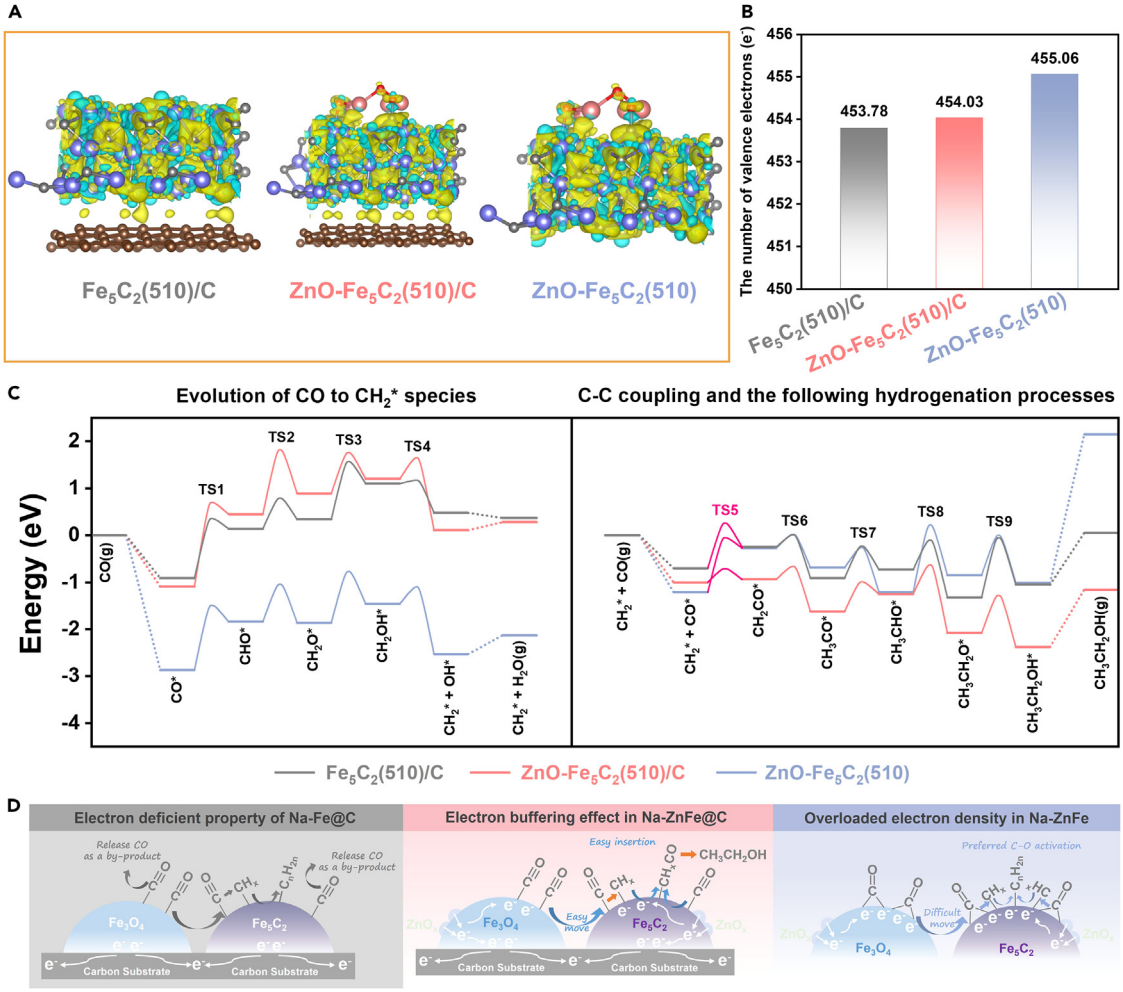

Figure 18. Theoretical simulation and mechanism analysis of ethanol synthesis via Fe-based catalysts

(A) Differential charge density plots of Fe_5C_2(510)/C, ZnO− Fe_5C_2 (510)/C, and ZnO− Fe_5C_2(510) models. The yellow and cyan electron clouds represent the accumulation and depletion of electrons, respectively.

(B) The valence electron number of Fe species in the three models.

(C) Energy profiles of −CO* species evolution, C−C coupling, and the following hydrogenation processes on the three models. Key: transition state (TS), Fe (purple), C (dark gray), Zn (yellow), O (red), H (white).

(D) Schematic diagram of the electron-buffering effect for ethanol synthesis from CO_2 hydrogenation. Reproduced with permission from Wang et al.[112] Copyright © 2023, John Wiley and Sons.

ambient temperature and converts it to CH_4 under mild conditions (250°C) in a dual-mode reactor. After five cycles, it stably captures 1.46 ± 0.24 mmol CO_2 g^{-1} and produces 1.52 ± 0.23 mmol CH_4 g^{-1}, similar sorbent-based catalysts reliant on the chemical looping of metal oxides and carbonates. This approach offers a new route for combined CO_2 capture and conversion using a dual-functional material for efficient low-temperature CO_2 desorption and CH_4 production.

MOFs' ordered and tunable properties make them promising precursors for CO_2 methanation catalysts. However, the role of promoters still needs to be explored. Li et al. developed a carbon-encapsulated NiFe alloy nanoparticle core-shell catalysts (Ni_xFe@C) prepared by impregnating Ni-MOF-74 in Fe^{3+} solution and subsequent pyrolysis.[119] Fe-doped catalysts showed enhanced CO_2 methanation activity over monometallic Ni, with Ni_7Fe@C achieving 72.3% CO_2 conversion and 99.3% CH_4 selectivity at 350°C. At 300°C, CO_2 conversion was 53.3%, double that of Ni@C. Experimental and DFT studies revealed that Fe incorporation improved metal particle dispersion, CO_2 and CO adsorption, leading to superior catalytic performance. This work offers a promising approach for the rational design of MOFs-derived CO_2 methanation catalysts and highlights the influence of promoters.

Regarding oxygen binding energy, Ru is one of the most promising catalysts for CO_2 methanation.[120] Recently, Loccufier et al. studied a catalytic membrane consisting of a silica nanofibrous structure as a carrier for Ru nanoparticles encapsulated within the MOFs Cr-MIL-101 (Figure 20).[121] This membrane was investigated for the Sabatier methanation reaction. Electrospinning of tetraorthosilicate (TEOS) sol

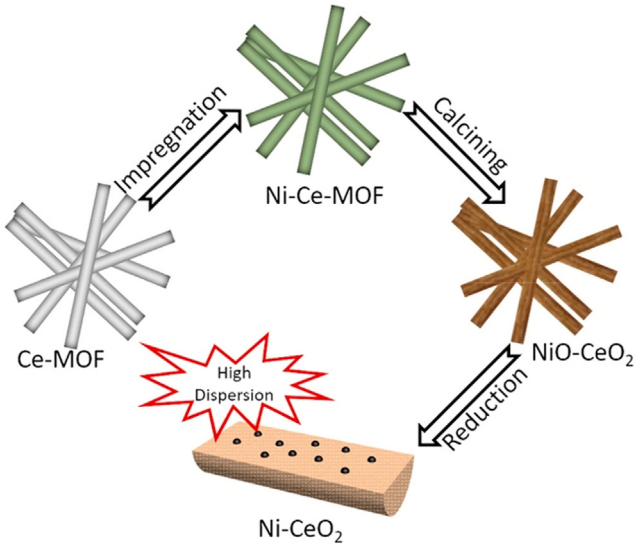

Figure 19. Simple illustration of the synthesis procedure of Ni/CeO_2.[117] Copyright © 2021, Elsevier

resulted in a thermally stable silica nanofibrous structure (up to 1100°C) with pores in the μm-range, enhancing gas throughput with reduced pressure requirements. A simple dip-coating method was used to deposit Ru@MIL-101 on the carrier, preventing Ru clustering. The catalytic membrane demonstrated an impressive turnover frequency of 3257 h^{-1} at 250°C, paving the way for structured reactors in efficient CO_2 hydrogenation processes. This system therefore paves the way toward structured reactors for efficient CO_2 hydrogenation processes.

It is well-established that MOFs-derived metal oxides often maintain the morphology of their precursor MOFs. However, Fan et al. demonstrated a novel approach to modulate the morphology of ZIF-67-derived Co_3O_4 from 3D dodecahedrons to 0D nanospheres by growing them over 1D TiO_2 nanowires (NWs).[122] This transformation is attributed to the disruption caused by the 1D TiO_2 NWs, which decompose the dodecahedral structure and disperse the Co_3O_4 nanoparticles. The nanocomposite Insitu-10N7CT achieves a high CO_2 conversion (97.42%) and CH_4 selectivity (99.29%), surpassing its mechanically assembled counterpart M−10N7CT (X_{CO2} = 91.45%, S_{CH4} = 98.42%). This enhancement is attributed to the intimate interfacial contact between the multi-dimensional Ni, 0D Co_3O_4, and 1D TiO_2 NWs, achieved by uniform dispersion of Co_3O_4 along the TiO_2 NWs. Due to the strong interfacial contact, metallic/metal oxide Ni-Co throughout the nanocomposite introduces additional oxygen vacancies, enhancing catalytic performance and potentially altering the methanation reaction mechanism.

In summary, MOFs-based catalysts exhibit both noteworthy advantages and challenges in the realm of CO_2 hydrogenation. Their primary advantage lies in the tunable nature of their structure, enabling precise engineering of the active site through the selection of metal ions and organic ligands. This design flexibility is pivotal in enhancing the catalytic activity and selectivity of the CO_2 hydrogenation. Furthermore, MOFs' exceptional surface area and porosity facilitate reactant diffusion and mass transfer, thereby boosting catalytic performance. However, stability remains a significant challenge for MOF-based catalysts, often trailing behind traditional catalysts. MOFs may collapse or decompose under harsh reaction conditions, such as elevated temperatures and pressures, limiting their widespread application in CO_2 hydrogenation. Thus, they are primarily utilized as sacrificial precursor. Additionally, the synthesis of MOFs is often intricate and costly, demanding precise control of reaction conditions and raw material ratios. In conclusion, while MOF-based catalysts offer unique advantages in CO_2 hydrogenation, their stability and synthesis cost remain key challenges that must be addressed for industrial scalability and widespread implementation.

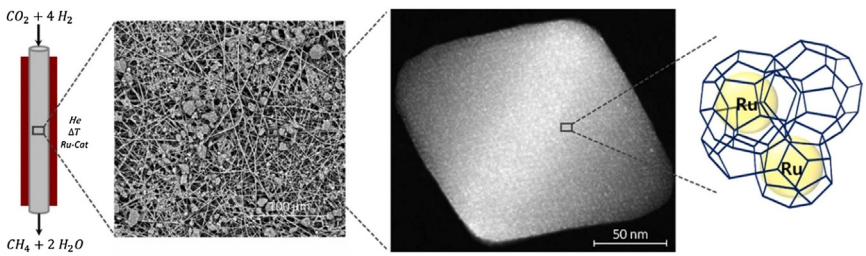

Figure 20. Scheme of the incorporation of silica nanofibrous veils as support for MIL-101 nanostructures loaded with Ru nanoparticles to catalyze the hydrogenation of CO_2 to CH_4.[121] Copyright © 2023, Elsevier

Table 4. Summary of MOFs-based catalysts for methane reforming

		Reaction condition					Conversion (%)			
Entry	Catalysts	GHSV[a] ($mL\ g^{-1}\ h^{-1}$)	Feed gas ratio	T (°C)	P (bar)	TOS (h)	CH_4	CO_2	H_2/CO	Reference
1	$NiAl_{MIL}$	72000	$CH_4:CO_2:Ar$ = 5/5/90	650	1	100	74.0	80.0	1.03	Karam et al., 2021[127]
2	Ni/Al_{MIL}	72000	$CH_4:CO_2:Ar$ = 5/5/90	650	1	13	70.0	77.0	1.09	Karam et al., 2021[127]
3	$NiCo@C/Al_2O_3$	60000	$CH_4:CO_2:N_2$ = 5/5/90	700	1	8	43.0	57.0	0.87	Liang et al., 2020[130]
4	$NiCo_2@C/Al_2O_3$	60000	$CH_4:CO_2:N_2$ = 5/5/90	700	1	8	35.0	41.0	0.80	Liang et al., 2020[130]
5	Ni-Co@CMOF-74	33000	$CH_4:CO_2:N_2$ = 1/1/1	700	5	10	49.0	58.0	–	Khan et al., 2021[131]
6	Ni-Co@CMOF-74	33000	$CH_4:CO_2:N_2$ = 1/1/1	750	5	10	60.0	69.0	0.82	Khan et al., 2021[131]
7	$Ni\text{-}MgO@mSiO_2^{MOF}$	36000	$CH_4:CO_2$ = 1/1	700	1	60	75.0	69.0	~0.87	Wang et al., 2022[132]
8	$Ni\text{-}MgO/mSiO_2^{NO3}$	36000	$CH_4:CO_2$ = 1/1	700	1	60	47.0	43.0	~0.82	Wang et al., 2022[132]
9	N_2-pyr	30000	$CH_4:CO_2:N_2$ = 1/1/2	700	1	24	70.0	83.0	0.98	Alli et al., 2023[133]
10	H_2-pyr	30000	$CH_4:CO_2:N_2$ = 1/1/2	700	1	24	58.0	77.0	0.91	Alli et al., 2023[133]
11	CO_2-pyr	30000	$CH_4:CO_2:N_2$ = 1/1/2	700	1	24	~56.0	~75.0	~0.90	Alli et al., 2023[133]
12	Ni/MCF	18000	$CH_4:CO_2:N_2$ = 1/1/2	600	1	25	~24.0	~34.0	~0.64	Shen et al., 2023[134]
13	Ni@C/MCF-650	18000	$CH_4:CO_2:N_2$ = 1/1/2	600	1	25	~21.0	31.0	~0.53	Shen et al., 2023[134]
14	Ni@C/MCF-750	18000	$CH_4:CO_2:N_2$ = 1/1/2	600	1	25	~48.0	52.4	~0.67	Shen et al., 2023[134]
15	$NiCeO_2@C\text{-}SIM$[b]	235200	$CH_4:CO_2:N_2$ = 8/8/180 H_2O (L) = 0.18 $mL\ h^{-1}$	600	1	8	48.0	17.0	1.4	Tu et al., 2023[135]
16	$NiCeO_2@C\text{-}IM$[b]	235200	$CH_4:CO_2:N_2$ = 8/8/180 H_2O (L) = 0.18 $mL\ h^{-1}$	600	1	8	40.1	11.8	1.4	Tu et al., 2023[135]

[a]Gas hourly space velocity.
[b]Catalytic performance of bi-reforming of methane (BRM).

METHANE CONVERSION

Methane (CH_4) is a crucial fossil fuel widely found in various sources such as natural gas, shale gas, coalbed methane, combustible ice, and biogas.[123] However, the highest C-H bond strength (434 $kJ\ mol^{-1}$) among all alkanes, coupled with the low polarizability and negligible electron affinity, makes CH_4 the least reactive alkane. Therefore, the activation and conversion of methane remain a long-standing challenge in catalysis despite the numerous material classes and process variants that have been explored.[124,125]

The primary strategies for methane conversion have been classified into two categories: the indirect routes via syngas and the direct conversion routes. The current industrial route for methane conversion is indirect. It primarily relies on reforming processes such as steam reforming methane (SRM), carbon dioxide (CO_2) reforming methane (CRM), and partial oxidation reforming methane (PORM). These processes generally require high pressure and high temperature. The direct methane conversion reactions mainly include partial oxidation of methane (POM), oxidative coupling of methane (OCM), and nonoxidative coupling of methane (NOCM). Direct methane conversion routes appear to be more favorable than reforming processes due to lower investment requirements, energy savings, and production costs. However, more efficient catalysts must be developed and utilized to improve their impractically low net yields of desired products. MOFs-based catalysts for POM and OCM have been reviewed elsewhere[24] and will not be included in this review. Metal/zeolite catalysts are widely used in NOCM, and a series of single-atom-based catalysts have been developed recently, but MOFs-based catalysts have yet to be reported.[126] Therefore, this section will mainly focus on the recent research progress of MOFs-based catalysts in methane reforming. The catalytic activities of several MOFs-based catalysts for methane reforming are summarized in Table 4.

The methane reforming process generally requires high-temperature oxidation to synthesize syngas. In this regard, direct methane reforming on the original MOFs catalyst seems impossible, given its thermal stability. Therefore, using MOFs as sacrificial templates or catalyst precursors to prepare MOFs-derived catalysts is the main strategy for the application of MOFs-based catalysts in methane reforming. As far as we know, in 2019, Karam et al. were the first to use MOFs-based materials for methane reforming.[127] The MIL-53 (1130 $m^2\ g^{-1}$) was used as a support precursor and a hard template, intimately mixed with the Ni precursor at the impregnation step, as depicted in Figure 21. The Al-OH groups and pores in the MOFs anchored the Ni precursor, and after a 500°C calcination in air, a porous Ni-Al solid solution formed. After reduction to a porous lamellar γ-Al_2O_3 material with small Ni nanoparticles homogeneously dispersed and stabilized within the support, leading to an outstanding catalytic stability with no activity loss during a 100 h reaction. This report revealed that MOFs could be used as a sacrificial template and porous host to stabilize metal species and obtain fine Ni particles. In addition, Karam et al. further compared another synthesis strategy of mesoporous Ni-alumina materials based on one-pot synthesis combined with the EISA method and summarized the critical characteristics of preparing efficient and stable Ni-aluminum catalysts for methane dry reforming.[128]

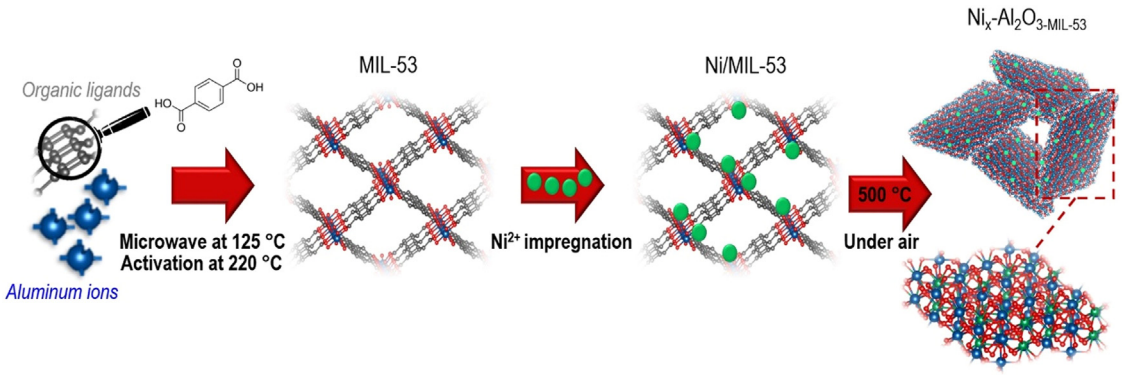

Figure 21. Schematic summarizing the MOFs-based preparation route of the Ni-alumina catalyst (Ni_x-$Al_2O_{3\text{-}MIL\text{-}53}$) Reproduced with permission from Karam et al.[128] Copyright © 2019, Multidisciplinary Digital Publishing Institute

In addition to synthesizing MOFs as supports and impregnating Ni, MOFs containing Ni can be directly synthesized and then pyrolyzed to obtain MOFs-derived catalysts. Leong et al. synthesized a series of NH_2-MIL-88B with varying molar ratios of Ni:Ce (2:1–1:2), showing high DRM activity.[129] The addition of Ce promoted a smaller particle size of Ni, ranging from 4.6 nm to 6.88 nm. Within the range of the studied molar ratios, 1Ni2Ce showed the highest CH_4 and CO_2 conversion at 63.5% and 86.8%, respectively, at 800°C, further supporting the promotion of Ce. In addition to NiCo MOFs, Leong et al. also attempted *in situ* growth of NiCo MOFs on Al_2O_3 support, followed by pyrolysis to obtain NiCo@C/Al_2O_3 catalyst.[130] The catalyst's basicity increases by incorporating Co into Ni. This enhancement boosts turnover frequencies, light-off stability, and operation stability toward catalytic dry reforming of methane. Gascon et al. also noted the possibility of Ni-Co bimetallic catalyst application in methane dry reforming.[131] They explored using MOF-74/CPO-27 as precursors for synthesizing Ni, Co, and bimetallic Ni-Co metal nanoparticles. The bimetallic Ni-Co@CMOF-74 catalyst showed better catalytic results than monometallic materials due to the synergistic effect of Ni and Co that impedes the coke formation.

Another bimetallic catalyst, Li et al., using MOFs/SiO_2 composite precursor synthesized mesoporous Ni-MgO solid solution catalyst Ni-MgO@$mSiO_2^{MOF}$ by one-pot calcination.[132] The chemical interaction between bimetallic Ni-Mg@H4DOT and $mSiO_2$ gel was confirmed by ^{29}Si and ^{13}C MAS NMR, demonstrating the successful synthesis of a Ni-MgO@$mSiO_2$ MOFs catalyst with outstanding catalytic activity, stability, and coke tolerance. This work is the first example of MOFs/SiO_2 composite with chemical interaction derived mesoporous silica confined Ni-MgO solid solution catalyst, which exhibits excellent performance and coke resistance for dry reforming of methane (DRM). The enhanced performance and coke resistance of the Ni-MgO@$mSiO_2$ MOFs catalyst can be attributed to the MOFs-templated strategy, which improves the dispersity of Ni species, enhances the interaction between Ni and Mg species, and inhibits the diffusion of Mg species into $mSiO_2$, thus preventing the formation of Mg_2SiO_4 and/or Mg-*O*-Si species. In addition, the MOFs/SiO_2 composite with chemical interaction serves as a precursor that improves the reduction degree of NiO and induces more reducible metallic Ni species with small size and strong metal-support interaction (SMSI) exsoluted from NiO-MgO-$mSiO_2$ compared with pristine NiO-MgO solid solution. Furthermore, the developed Ni-MgO@$mSiO_2$ MOFs catalysts exhibit higher reactant adsorption ability and accelerate the generation of more OH* species on the surface of the catalyst, which contributes to the elimination of coke during the reaction process.

Different pyrolysis processes after MOFs synthesis also greatly influence the catalytic performance. Mahinpey et al. developed a novel catalyst synthesis scheme using a bimetallic Ni-Ce-BTC MOFs template to synthesize nanostructured Ni/CeO_2 catalysts.[133] Three different environments were used to remove the organic template during the thermal process. In addition, further catalyst thermal pre-treatment under a CO_2 environment was performed. The study results indicate that the catalyst labeled N_2-pyr, which underwent only heat treatment under nitrogen, exhibited the most favorable activity and higher stability. This catalyst showed no decline in activity after 24 h on stream, with CO_2 and CH_4 conversions of 83% and 70%, respectively. Meanwhile the catalysts treated thermally under a CO_2 atmosphere presented the lowest activity, attributed to weaker metal-support interaction, lesser dispersion, larger crystallite size (>10 nm), lesser Ce^{3+}, and surface oxygen. These factors can influence the reducibility of the catalyst and its activity. Additionally, a stability test was carried out on the N_2-pyr catalyst for 120 h (5 days) on stream, and the results showed no catalyst deactivation or decline in activity or stability.

Methane dry reforming requires a high reaction temperature (generally above 700°C), and lower temperatures usually result in severe carbon deposition. Wang et al. successfully synthesized a carbon-confined Ni@C/MCF catalyst by carbonizing MOFs on MCF supports.[134] During the carbonization process in a N_2 flow, metallic Ni NPs were formed without needing a separate H_2 reduction step. The Ni@C/MCF-750 catalyst exhibited excellent catalytic performance at 600°C. The carbon layers effectively protected the Ni NPs from sintering and coking due to the confinement effect, thus effectively mitigating the challenges of deactivation caused by sintering and coking in DRM reactions.

MOFs-based catalysts can also be used for the bi-reforming of methane (BRM). Kung et al. incorporate catalytically active nickel into highly porous cerium(IV)-based MOFs using either conventional impregnation techniques or self-limiting post-synthetic modifications.[135] Subsequently, nanosized MOFs-derived ceria-supported nickel is prepared by carbonizing nickel-incorporated Ce-based MOFs. The crystallinity, porosity, nanostructural morphology, and surface properties of each MOFs and the resulting MOFs-derived materials are meticulously characterized, and as a demonstration, the MOFs-derived catalysts are used for BRM.

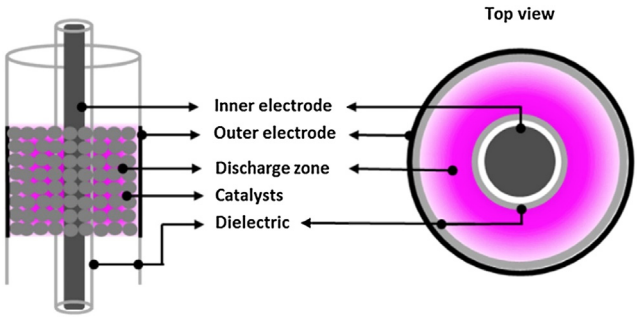

Figure 22. Schematic diagram of the DBD plasma-catalytic reactor
Reproduced with permission from Vakili et al.[136] Copyright © 2020, Elsevier.

Certain conditions enable MOFs materials to serve as both chemically and thermodynamically stable supports. By loading PtNPs onto UiO-67, Vakili et al. achieved a plasma-assisted dry reforming process that transcended the thermodynamic limitations of dry reforming reactions. (Figure 22).[136] This breakthrough relies on the utilization of energetic electrons to activate reactive molecules rather than traditional thermal activation methods. The UiO-67, with exceptional porosity and surface area exceeding 2000 m^2 g^{-1}, exhibits exceptional stability under plasma conditions and promotes optimal dispersion of platinum particles. Furthermore, UiO-67 promotes plasma formation and surface discharges in the discharge zone, synergistically enhancing the conversion of CH_4 and CO_2 and syngas production.

In conclusion, research on the catalytic conversion of methane using MOFs-based materials has only recently begun, and there are relatively few related reports. Compared with other leading catalysts such as zeolites, metal oxides, and metal alloys, there are still significant gaps in the stability and activity of MOFs-based catalysts. However, from the existing reports, the prospects for MOFs-based catalysts are still up and coming. MOFs materials possess several unique intrinsic features not found in other materials, making them particularly advantageous in catalyst design.

CONCLUSIONS AND PERSPECTIVE

In this review, we provide a brief overview of the existing state of the art on using MOFs and MOFs-derived materials as catalysts or supports for C1 catalysis to produce valuable chemicals. As a relatively new class of porous materials, MOFs have attracted significant interest due to their high surface area, chemical versatility, and structural diversity. At the end of this review, we want to identify key technical challenges and suggest future research directions for MOFs and their derivates for the thermal-catalytic conversion of C1 molecules.

First and foremost, the poor stability of MOFs limits their practical application in C1 catalysis. The instability of MOFs can be attributed to the decomposition of their chemical structure under harsh conditions, making them unsuitable for long-term use. Currently, most research aims to produce MOFs-derived materials with higher thermal stability through thermal decomposition treatment. However, the thermal treatment process often sacrifices many of the properties and functions of the original MOFs. To address this challenge, exploring synthetic methods for more stable MOFs or advanced post-synthetic modifications that preserve the original characteristics of MOFs while enhancing their stability is essential. Additionally, utilizing more advanced reaction processes, such as plasma-assisted methods, to replace traditional thermal processes and maintain the stability of MOFs-based materials during reactions is a promising approach.

Secondly, the practical application of MOFs-based catalysts is challenging due to the difficulties in shaping them into particles with micron or centimeter-scale diameter. In practical reactions, especially in fixed-bed reactors, catalysts often need to be formulated into pellets or monoliths to achieve better mass and heat transfer. However, existing MOFs-based catalysts often exist as carbonaceous powders, making it challenging to architect them into suitable shapes. This problem can be addressed by exploring different shaping methods for MOFs-based catalysts. By employing novel techniques such as 3D printing, it may be possible to enhance the mechanical strength and durability of MOFs-based catalysts, making them more suitable for practical applications.

Additionally, utilizing MOFs as precursors for the preparation of bimetallic or trimetallic catalysts is a promising research direction in MOFs-based C1 catalysts. By combining different metals in a single catalyst, it may be possible to achieve improved catalytic activity and selectivity for the conversion of C1 molecules. This approach may provide a more cost-effective and sustainable alternative to traditional catalyst preparation methods. It could open up new avenues for the development of novel MOFs-based catalysts for C1 catalysis.

Finally, it is important to collaborate and share knowledge across different research fields to promote the development of MOFs-based catalysts for converting C1 resources into clean fuels or valuable chemicals. This collaboration can lead to innovative solutions and new applications in this field. For example, the expert with plentiful materials synthesis experience could increase the yield of MOFs high enough for ton-scale industrial application. During the large-scale synthesis process, chemical engineering issues should be considered thoroughly to ensure the uniform and stable crystal growth.

Even though many challenges remain and our understanding of these porous materials is still incomplete, it is believed that the design and synthesis of more functional MOFs materials with specific properties will promote the rapid development of C1 chemistry in the near future. We hope this review will provide valuable insights and suggestions for future research in this area.

ACKNOWLEDGMENTS

This work was supported by the National Key Research and Development Program of China (2023YFB4104500, 2023YFB4104502), National Natural Science Foundation of China (22108310), the Science and Technology Innovation Project of the Shandong Energy Group Co., Ltd. (SNKJ2023A03).

AUTHOR CONTRIBUTIONS

S.Y.L.: Writing-Original Draft and Editing, Visualization. Y.J. C.: Writing-Original Draft and Editing, Visualization. H.Y.L.: Writing-Original Draft and Editing, Visualization. W.H.W.: Writing-Review & Editing. Y.W.: Writing-Review and Editing, Project administration. M.B. W.: Project administration.

DECLARATION OF INTERESTS

The authors declare no competing interests.

REFERENCES

1. Liu, Y., Deng, D., and Bao, X. (2020). Catalysis for selected C1 chemistry. Chem *6*, 2497–2514.
2. Mesters, C. (2016). A selection of recent advances in C1 chemistry. Annu. Rev. Chem. Biomol. Eng. *7*, 223–238.
3. Wang, Y., Sun, J., and Tsubaki, N. (2023). Clever nanomaterials fabrication techniques encounter sustainable C1 catalysis. Acc. Chem. Res. *56*, 2341–2353.
4. Wang, W., Ma, Z., Fei, X., Wang, X., Yang, Z., Wang, Y., Zhang, J., Ning, H., Tsubaki, N., and Wu, M. (2022). Joint tuning the morphology and oxygen vacancy of Cu_2O by ionic liquid enables high-efficient CO_2 reduction to C_2 products. Chem. Eng. J. *436*, 135029.
5. Wang, W., Wang, X., Ma, Z., Wang, Y., Yang, Z., Zhu, J., Lv, L., Ning, H., Tsubaki, N., and Wu, M. (2023). Carburized In_2O_3 nanorods endow CO_2 electroreduction to formate at 1 A cm^{-2}. ACS Catal. *13*, 796–802.
6. Jiao, F., Li, J., Pan, X., Xiao, J., Li, H., Ma, H., Wei, M., Pan, Y., Zhou, Z., Li, M., et al. (2016). Selective conversion of syngas to light olefins. Science *351*, 1065–1068.
7. Wei, J., Ge, Q., Yao, R., Wen, Z., Fang, C., Guo, L., Xu, H., and Sun, J. (2017). Directly converting CO_2 into a gasoline fuel. Nat. Commun. *8*, 15174.
8. Shan, J., Li, M., Allard, L.F., Lee, S., and Flytzani-Stephanopoulos, M. (2017). Mild oxidation of methane to methanol or acetic acid on supported isolated rhodium catalysts. Nature *551*, 605–608.
9. Zhou, H.C.J., and Kitagawa, S. (2014). Metal–organic frameworks (MOFs). Chem. Soc. Rev. *43*, 5415–5418.
10. Kitao, T., Zhang, Y., Kitagawa, S., Wang, B., and Uemura, T. (2017). Hybridization of MOFs and polymers. Chem. Soc. Rev. *46*, 3108–3133.
11. Zhou, H.-C., Long, J.R., and Yaghi, O.M. (2012). Introduction to Metal–Organic Frameworks. Chem. Rev. *112*, 673–674.
12. Li, H., Eddaoudi, M., O'Keeffe, M., and Yaghi, O.M. (1999). Design and synthesis of an exceptionally stable and highly porous metal-organic framework. Nature *402*, 276–279.
13. Xu, W., Thapa, K.B., Ju, Q., Fang, Z., and Huang, W. (2018). Heterogeneous catalysts based on mesoporous metal–organic frameworks. Coord. Chem. Rev. *373*, 199–232.
14. Eddaoudi, M., Sava, D.F., Eubank, J.F., Adil, K., and Guillerm, V. (2015). Zeolite-like metal–organic frameworks (ZMOFs): design, synthesis, and properties. Chem. Soc. Rev. *44*, 228–249.
15. Cohen, S.M. (2012). Postsynthetic methods for the functionalization of metal–organic frameworks. Chem. Rev. *112*, 970–1000.
16. Guo, J., Lian, Y., Li, F., Duan, Y., Xue, X., Long, C., Zhang, Y., and Tang, Z. (2022). Metal-organic frameworks' tricks in asymmetric catalysis. Chem Catal. *2*, 2986–3018.
17. Guo, J., Duan, Y., Jia, Y., Zhao, Z., Gao, X., Liu, P., Li, F., Chen, H., Ye, Y., Liu, Y., et al. (2024). Biomimetic chiral hydrogen-bonded organic-inorganic frameworks. Nat. Commun. *15*, 139.
18. Furukawa, H., Go, Y.B., Ko, N., Park, Y.K., Uribe-Romo, F.J., Kim, J., O'Keeffe, M., and Yaghi, O.M. (2011). Isoreticular expansion of metal–organic frameworks with triangular and square building units and the lowest calculated density for porous crystals. Inorg. Chem. *50*, 9147–9152.
19. Deng, H., Grunder, S., Cordova, K.E., Valente, C., Furukawa, H., Hmadeh, M., Gándara, F., Whalley, A.C., Liu, Z., Asahina, S., et al. (2012). Large-pore apertures in a series of metal-organic frameworks. Science *336*, 1018–1023.
20. O'Keeffe, M. (2009). Design of MOFs and intellectual content in reticular chemistry: a personal view. Chem. Soc. Rev. *38*, 1215–1217.
21. Otun, K.O., Liu, X., and Hildebrandt, D. (2020). Metal-organic framework (MOF)-derived catalysts for Fischer-Tropsch synthesis: Recent progress and future perspectives. J. Energy Chem. *51*, 230–245.
22. Wang, H. (2022). Nanostructure@metal-organic frameworks (MOFs) for catalytic carbon dioxide (CO_2) conversion in photocatalysis, electrocatalysis, and thermal catalysis. Nano Res. *15*, 2834–2854.
23. Modak, A., Ghosh, A., Bhaumik, A., and Chowdhury, B. (2021). CO_2 hydrogenation over functional nanoporous polymers and metal-organic frameworks. Adv. Colloid Interface Sci. *290*, 102349.
24. Andrade, L.S., Lima, H.H., Silva, C.T., Amorim, W.L., Poço, J.G., López-Castillo, A., Kirillova, M.V., Carvalho, W.A., Kirillov, A.M., and Mandelli, D. (2023). Metal-organic frameworks as catalysts and biocatalysts for methane oxidation: The current state of the art. Coord. Chem. Rev. *481*, 215042.
25. Fan, W.K., and Tahir, M. (2021). Current trends and approaches to boost the performance of metal organic frameworks for carbon dioxide methanation through photo/thermal hydrogenation: A review. Ind. Eng. Chem. Res. *60*, 13149–13179.
26. Cui, W.-G., Zhang, G.-Y., Hu, T.-L., and Bu, X.-H. (2019). Metal-organic framework-based heterogeneous catalysts for the conversion of C1 chemistry: CO, CO_2 and CH_4. Coord. Chem. Rev. *387*, 79–120.
27. van Spronsen, M.A., Frenken, J.W.M., and Groot, I.M.N. (2017). Surface science under reaction conditions: CO oxidation on Pt and Pd model catalysts. Chem. Soc. Rev. *46*, 4347–4374.
28. Wang, T., Gao, L., Hou, J., Herou, S.J.A., Griffiths, J.T., Li, W., Dong, J., Gao, S., Titirici, M.-M., Kumar, R.V., et al. (2019). Rational approach to guest confinement inside MOF cavities for low-temperature catalysis. Nat. Commun. *10*, 1340.
29. Cheng, K., Zhou, W., Kang, J., He, S., Shi, S., Zhang, Q., Pan, Y., Wen, W., and Wang, Y. (2017). Bifunctional catalysts for one-step conversion of syngas into aromatics with excellent selectivity and stability. Chem *3*, 334–347.
30. Torres Galvis, H.M., and de Jong, K.P. (2013). Catalysts for production of lower olefins from synthesis gas: A review. ACS Catal. *3*, 2130–2149.
31. An, Y., Lin, T., Yu, F., Yang, Y., Zhong, L., Wu, M., and Sun, Y. (2017). Advances in direct production of value-added chemicals via syngas conversion. Sci. China Chem. *60*, 887–903.
32. Li, F., Ao, M., Pham, G.H., Sunarso, J., Chen, Y., Liu, J., Wang, K., and Liu, S. (2020). Cu/ZnO catalysts derived from bimetallic metal–organic framework for dimethyl ether synthesis from syngas with enhanced selectivity and stability. Small *16*, 1906276.
33. Guo, Y., Feng, L., Liu, Y., and Zhao, Z. (2022). Cu-embedded porous Al_2O_3 bifunctional catalyst derived from metal–organic framework for syngas-to-dimethyl ether. Chin. Chem. Lett. *33*, 2906–2910.
34. Zhang, Z., Huang, Y., Ma, H., Qian, W., Zhang, H., and Ying, W. (2021). Syngas-to-olefins over MOF-derived $ZnZrO_x$ and SAPO-34 bifunctional catalysts. Catal. Commun. *152*, 106292.
35. Yu, J., Li, G., Han, Y., Zheng, X., Mao, H., and Mao, D. (2022). Comparative study on ethanol-based oxygenate synthesis via syngas over Rh–Mn bimetallic catalysts supported on different UiO MOFs. Energy Fuels *36*, 11940–11949.

36. Santos, V.P., Wezendonk, T.A., Jaén, J.J.D., Dugulan, A.I., Nasalevich, M.A., Islam, H.-U., Chojecki, A., Sartipi, S., Sun, X., Hakeem, A.A., et al. (2015). Metal organic framework-mediated synthesis of highly active and stable Fischer-Tropsch catalysts. Nat. Commun. *6*, 6451.
37. Sun, X., Suarez, A.I.O., Meijerink, M., van Deelen, T., Ould-Chikh, S., Zečević, J., de Jong, K.P., Kapteijn, F., and Gascon, J. (2017). Manufacture of highly loaded silica-supported cobalt Fischer–Tropsch catalysts from a metal organic framework. Nat. Commun. *8*, 1680.
38. Isaeva, V.I., Eliseev, O.L., Kazantsev, R.V., Chernyshev, V.V., Davydov, P.E., Saifutdinov, B.R., Lapidus, A.L., and Kustov, L.M. (2016). Fischer–Tropsch synthesis over MOF-supported cobalt catalysts (Co@MIL-53(Al)). Dalton Trans. *45*, 12006–12014.
39. Cui, W.-G., Li, Y.-T., Zhang, H., Wei, Z.-C., Gao, B.-H., Dai, J.-J., and Hu, T.-L. (2020). In situ encapsulated Co/MnO_x nanoparticles inside quasi-MOF-74 for the higher alcohols synthesis from syngas. Appl. Catal. B Environ. *278*, 119262.
40. Lü, B., Qi, W., Luo, M., Liu, Q., and Guo, L. (2020). Fischer–Tropsch synthesis: ZIF-8@ZIF-67-derived cobalt nanoparticle-embedded nanocage catalysts. Ind. Eng. Chem. Res. *59*, 12352–12359.
41. Luo, Q.-X., Guo, L.-P., Yao, S.-Y., Bao, J., Liu, Z.-T., and Liu, Z.-W. (2019). Cobalt nanoparticles confined in carbon matrix for probing the size dependence in Fischer-Tropsch synthesis. J. Catal. *369*, 143–156.
42. Chen, Y., Li, X., Zhang, J., Dai, L., Zhao, N., Liu, C., Lyu, S., and Li, Z. (2021). Insight into the influence of the graphite layer and cobalt crystalline on a ZIF-67-derived catalyst for Fischer–Tropsch synthesis. ACS Appl. Mater. Interfaces *13*, 9885–9896.
43. Chen, Y., Li, X., Zhang, J., Zhao, N., Dai, L., Jiang, X., Liu, C., Lyu, S., and Li, Z. (2021). Preparation of SiO_2 immobilized Co-based catalysts from ZIF-67 and the enhancement effect for Fischer-Tropsch synthesis. Appl. Catal. B Environ. *289*, 120027.
44. Chen, Y., Li, X., Dai, L., Nisa, M.U., Liu, C., Lv, S., Lv, J., and Li, Z. (2020). Controllable synthesis of core-shell Co@C@SiO_2 catalysts for enhancing product selectivity in Fischer-Tropsch synthesis by tuning the mass transfer resistance. J. Energy Chem. *51*, 199–206.
45. Zhao, N., Chen, Y., Li, X., Nisa, M.U., Jiang, X., Dai, L., and Li, Z. (2021). Preparation of high performance Co_3O_4/Al_2O_3 catalysts by doping Al into ZIF-67: Effect of Al sources on Fischer-Tropsch synthesis. Appl. Surf. Sci. *570*, 151127.
46. Qin, C., Bai, J., Xu, Y., Du, Y., Wang, J., and Ding, M. (2022). A high active sites exposed hollow Co@SiO_2 nanoreactor for high performance fischer–tropsch synthesis. Fuel *323*, 124377.
47. Qin, H., Zhou, Y., Huang, Q., Yang, Z., Dong, R., Li, L., Tang, J., Zhang, C., and Jiang, F. (2021). Metal organic framework (MOF)/wood derived multi-cylinders high-power 3D reactor. ACS Appl. Mater. Interfaces *13*, 5460–5468.
48. Girardon, J., Lermontov, A., Gengembre, L., Chernavskii, P., Griboval-Constant, A., and Khodakov, A. (2005). Effect of cobalt precursor and pretreatment conditions on the structure and catalytic performance of cobalt silica-supported Fischer–Tropsch catalysts. J. Catal. *230*, 339–352.
49. Munnik, P., Velthoen, M.E.Z., de Jongh, P.E., de Jong, K.P., and Gommes, C.J. (2014). Nanoparticle growth in supported nickel catalysts during methanation reaction—larger is better. Angew. Chem. Int. Ed. *53*, 9493–9497.
50. Munnik, P., Krans, N.A., de Jongh, P.E., and de Jong, K.P. (2014). Effects of drying conditions on the synthesis of Co/SiO_2 and Co/Al_2O_3 Fischer–Tropsch catalysts. ACS Catal. *4*, 3219–3226.
51. Luo, M., Li, M., Lü, B., Liu, Q., Di, Z., and Guo, L. (2021). Cobalt nanoparticle-decorated LDH/ZIF-derived porous nanoplatelets for Fischer–Tropsch synthesis. ACS Appl. Nano Mater. *4*, 3734–3741.
52. Subramanian, N.D., Balaji, G., Kumar, C.S., and Spivey, J.J. (2009). Development of cobalt–copper nanoparticles as catalysts for higher alcohol synthesis from syngas. Catal. Today *147*, 100–106.
53. Ao, M., Pham, G.H., Sunarso, J., Tade, M.O., and Liu, S. (2018). Active centers of catalysts for higher alcohol synthesis from syngas: A review. ACS Catal. *8*, 7025–7050.
54. Li, F., Li, J., Wang, K., Ao, M., Qiu, J., Zhang, X., Wang, H., Pham, G.H., and Liu, S. (2021). Co/Co_6Mo_6C@C nanoreactors derived from ZIF-67 composite for higher alcohols synthesis. Compos. Part B Eng. *209*, 108608.
55. Guo, S., Li, Z., Li, Y., Zeng, Z., Lv, J., Huang, S., Wang, Y., and Ma, X. (2023). CoMn catalysts derived from partial decomposed layered CoMn-MOF materials for higher alcohol synthesis from syngas. Chem. Eng. J. *463*, 142359.
56. Jin, Y., and Datye, A.K. (2000). Phase transformations in iron Fischer–Tropsch catalysts during temperature-programmed reduction. J. Catal. *196*, 8–17.
57. Cheng, X., Yang, H., and Tatarchuk, B.J. (2016). Microfibrous entrapped hybrid iron-based catalysts for Fischer–Tropsch synthesis. Catal. Today *273*, 62–71.
58. Zhao, D., Shui, J.-L., Chen, C., Chen, X., Reprogle, B.M., Wang, D., and Liu, D.-J. (2012). Iron imidazolate framework as precursor for electrocatalysts in polymer electrolyte membrane fuel cells. Chem. Sci. *3*, 3200–3205.
59. Zhang, H., Wang, Y., Zhao, W., Zou, M., Chen, Y., Yang, L., Xu, L., Wu, H., and Cao, A. (2017). MOF-derived ZnO nanoparticles covered by N-doped carbon layers and hybridized on carbon nanotubes for Lithium-Ion battery anodes. ACS Appl. Mater. Interfaces *9*, 37813–37822.
60. Cho, J.M., Kim, B.-G., Han, G.Y., Sun, J., Jeong, H.-K., and Bae, J.W. (2020). Effects of metal-organic framework-derived iron carbide phases for CO hydrogenation activity to hydrocarbons. Fuel *281*, 118779.
61. Rashed, A.E., Nasser, A., Elkady, M.F., Matsushita, Y., and El-Moneim, A.A. (2022). Fe nanoparticle size control of the Fe-MOF-derived catalyst using a solvothermal method: Effect on FTS activity and olefin production. ACS Omega *7*, 8403–8419.
62. Mehar, U.N., Chen, Y., Li, X., and Li, Z. (2020). Highly efficient iron based MOFs mediated catalysts for Fischer–Tropsch synthesis: Effect of reduction atmosphere. J. Taiwan Inst. Chem. Eng. *107*, 44–53.
63. Campisi, S., Chan-Thaw, C., and Villa, A. (2018). Understanding heteroatom-mediated metal–support interactions in functionalized carbons: A perspective review. Appl. Sci. *8*, 1159.
64. Cheng, Q., Zhao, N., Lyu, S., Tian, Y., Gao, F., Dong, L., Jiang, Z., Zhang, J., Tsubaki, N., and Li, X. (2019). Tuning interaction between cobalt catalysts and nitrogen dopants in carbon nanospheres to promote Fischer-Tropsch synthesis. Appl. Catal. B Environ. *248*, 73–83.
65. Xiong, H., Moyo, M., Motchelaho, M.A., Tetana, Z.N., Dube, S.M., Jewell, L.L., and Coville, N.J. (2014). Fischer–Tropsch synthesis: Iron catalysts supported on N-doped carbon spheres prepared by chemical vapor deposition and hydrothermal approaches. J. Catal. *311*, 80–87.
66. Zhao, Q., Huang, S., Han, X., Chen, J., Wang, J., Rykov, A., Wang, Y., Wang, M., Lv, J., and Ma, X. (2021). Highly active and controllable MOF-derived carbon nanosheets supported iron catalysts for Fischer-Tropsch synthesis. Carbon *173*, 364–375.
67. Munir, S., Amin, M., Iqbal, N., Iqbal, A., and Ghfar, A.A. (2023). Effect of pyrolysis on iron-metal organic frameworks (MOFs) to Fe_3C @ Fe_5C_2 for diesel production in Fischer-Tropsch synthesis. Front. Chem. *11*, 1150565.
68. Wang, A., Luo, M., Lü, B., Song, Y., Li, M., and Yang, Z. (2021). Effect of Na, Cu and Ru on metal-organic framework-derived porous carbon supported iron catalyst for Fischer-Tropsch synthesis. Mol. Catal. *509*, 111601.
69. Wang, A., Luo, M., Lü, B., Song, Y., Yang, Z., Li, M., Shi, B., and Khan, I. (2022). MOF-derived porous carbon-supported bimetallic Fischer–Tropsch synthesis catalysts. Ind. Eng. Chem. Res. *61*, 3941–3951.
70. Lu, W.-Z., Teng, L.-H., and Xiao, W.-D. (2004). Simulation and experiment study of dimethyl ether synthesis from syngas in a fluidized-bed reactor. Chem. Eng. Sci. *59*, 5455–5464.
71. Sun, K., Lu, W., Qiu, F., Liu, S., and Xu, X. (2003). Direct synthesis of DME over bifunctional catalyst: surface properties and catalytic performance. Appl. Catal. Gen. *252*, 243–249.
72. Bayat, A., and Dogu, T. (2016). Optimization of CO_2/CO ratio and temperature for dimethyl ether synthesis from syngas over a new bifunctional catalyst pair containing heteropolyacid impregnated mesoporous alumina. Ind. Eng. Chem. Res. *55*, 11431–11439.
73. Wang, Y., Zhan, W., Chen, Z., Chen, J., Li, X., and Li, Y. (2020). Advanced 3D hollow-out ZnZrO@C combined with hierarchical zeolite for highly active and selective CO hydrogenation to aromatics. ACS Catal. *10*, 7177–7187.
74. Zhong, L., Yu, F., An, Y., Zhao, Y., Sun, Y., Li, Z., Lin, T., Lin, Y., Qi, X., Dai, Y., et al. (2016). Cobalt carbide nanoprisms for direct production of lower olefins from syngas. Nature *538*, 84–87.
75. Torres Galvis, H.M., Bitter, J.H., Khare, C.B., Ruitenbeek, M., Dugulan, A.I., and de Jong, K.P. (2012). Supported iron nanoparticles as catalysts for sustainable production of lower olefins. Science *335*, 835–838.
76. Luk, H.T., Mondelli, C., Ferré, D.C., Stewart, J.A., and Pérez-Ramírez, J. (2017). Status and prospects in higher alcohols synthesis from syngas. Chem. Soc. Rev. *46*, 1358–1426.

77. Rungtaweevoranit, B., Baek, J., Araujo, J.R., Archanjo, B.S., Choi, K.M., Yaghi, O.M., and Somorjai, G.A. (2016). Copper nanocrystals encapsulated in Zr-based metal–organic frameworks for highly selective CO_2 hydrogenation to methanol. Nano Lett. *16*, 7645–7649.
78. Candian Firmino Marcos, F., Fonseca Costa, M.J., L. Catuzo, G., Angeli de Moraes, D., de Oliveira Junior, M., Mastelaro, V.R., Mansur Assaf, J., Giudici, R., and Moreira Assaf, E. (2023). Supported Cu catalysts on UiO-66 toward enhanced methanol selectivity by CO_2 hydrogenation: Effect of Cu loading. J. Catal. *427*, 115104.
79. Zhu, Y., Zheng, J., Ye, J., Cui, Y., Koh, K., Kovarik, L., Camaioni, D.M., Fulton, J.L., Truhlar, D.G., Neurock, M., et al. (2020). Copper-zirconia interfaces in UiO-66 enable selective catalytic hydrogenation of CO_2 to methanol. Nat. Commun. *11*, 5849.
80. Yang, Y., Xu, Y., Ding, H., Yang, D., Cheng, E., Hao, Y., Wang, H., Hong, Y., Su, Y., Wang, Y., et al. (2021). Cu/ZnO_x@UiO-66 synthesized from a double solvent method as an efficient catalyst for CO_2 hydrogenation to methanol. Catal. Sci. Technol. *11*, 4367–4375.
81. Mitsuka, Y., Ogiwara, N., Mukoyoshi, M., Kitagawa, H., Yamamoto, T., Toriyama, T., Matsumura, S., Haneda, M., Kawaguchi, S., Kubota, Y., and Kobayashi, H. (2021). Fabrication of integrated copper-based nanoparticles/amorphous metal–organic framework by a facile spray-drying method: Highly enhanced CO_2 hydrogenation activity for methanol synthesis. Angew. Chem. Int. Ed. *60*, 22283–22288.
82. Zhang, L., Cui, J., Zhang, Y., San, X., and Meng, D. (2023). Surface conversion of CuO–ZnO to ZIF-8 to enhance CO_2 adsorption for CO_2 hydrogenation to methanol. New J. Chem. *47*, 6700–6707.
83. Gutterød, E.S., Pulumati, S.H., Kaur, G., Lazzarini, A., Solemsli, B.G., Gunnæs, A.E., Ahoba-Sam, C., Kalyva, M.E., Sannes, J.A., Svelle, S., et al. (2020). Influence of Defects and H_2O on the Hydrogenation of CO_2 to Methanol over Pt Nanoparticles in UiO-67 Metal–Organic Framework. J. Am. Chem. Soc. *142*, 17105–17118.
84. Zhang, J., An, B., Cao, Y., Li, Z., Chen, J., He, X., and Wang, C. (2021). ZnO supported on a Zr-based metal–organic framework for selective CO_2 hydrogenation to methanol. ACS Appl. Energy Mater. *4*, 13567–13574.
85. Duma, Z.G., Moma, J., Langmi, H.W., Louis, B., Parkhomenko, K., and Musyoka, N.M. (2022). Towards high CO_2 conversions using Cu/Zn catalysts supported on aluminum fumarate metal-organic framework for methanol synthesis. Catalysts *12*, 1104.
86. Jiang, H.-L., Liu, B., Lan, Y.-Q., Kuratani, K., Akita, T., Shioyama, H., Zong, F., and Xu, Q. (2011). From metal–organic framework to nanoporous carbon: Toward a very high surface area and hydrogen uptake. J. Am. Chem. Soc. *133*, 11854–11857.
87. Pustovarenko, A., Dikhtiarenko, A., Bavykina, A., Gevers, L., Ramírez, A., Russkikh, A., Telalovic, S., Aguilar, A., Hazemann, J.-L., Ould-Chikh, S., and Gascon, J. (2020). Metal–organic framework-derived synthesis of cobalt indium catalysts for the hydrogenation of CO_2 to methanol. ACS Catal. *10*, 5064–5076.
88. Yu, J., Liu, S., Mu, X., Yang, G., Luo, X., Lester, E., and Wu, T. (2021). Cu-ZrO_2 catalysts with highly dispersed Cu nanoclusters derived from ZrO_2@ HKUST-1 composites for the enhanced CO_2 hydrogenation to methanol. Chem. Eng. J. *419*, 129656.
89. San, X., Gong, X., Hu, Y., Hu, Y., Wang, G., Qi, J., Meng, D., and Jin, Q. (2021). Highly dispersed Cu/graphene nanocatalyst guided by MOF structure: Application to methanol synthesis from CO_2 Hydrogenation. ChemistrySelect *6*, 6115–6118.
90. Qi, T., Zhao, Y., Chen, S., Li, W., Guo, X., Zhang, Y., and Song, C. (2021). Bimetallic metal organic framework-templated synthesis of a Cu-ZnO/Al_2O_3 catalyst with superior methanol selectivity for CO_2 hydrogenation. Mol. Catal. *514*, 111870.
91. Cai, Z., Huang, M., Dai, J., Zhan, G., Sun, F.-l., Zhuang, G.-L., Wang, Y., Tian, P., Chen, B., Ullah, S., et al. (2022). Fabrication of Pd/In_2O_3 nanocatalysts derived from MIL-68(In) loaded with molecular metalloporphyrin (TCPP(Pd)) toward CO_2 hydrogenation to methanol. ACS Catal. *12*, 709–723.
92. Han, X., Li, M., Chang, X., Hao, Z., Chen, J., Pan, Y., Kawi, S., and Ma, X. (2022). Hollow structured Cu@ZrO_2 derived from Zr-MOF for selective hydrogenation of CO_2 to methanol. J. Energy Chem. *71*, 277–287.
93. Hu, J., Yu, L., Deng, J., Wang, Y., Cheng, K., Ma, C., Zhang, Q., Wen, W., Yu, S., Pan, Y., et al. (2021). Sulfur vacancy-rich MoS_2 as a catalyst for the hydrogenation of CO_2 to methanol. Nat. Catal. *4*, 242–250.
94. Zhou, H., Chen, Z., López, A.V., López, E.D., Lam, E., Tsoukalou, A., Willinger, E., Kuznetsov, D.A., Mance, D., Kierzkowska, A., et al. (2021). Engineering the Cu/Mo_2CTx (MXene) interface to drive CO_2 hydrogenation to methanol. Nat. Catal. *4*, 860–871.
95. Zhou, S., Ma, W., Anjum, U., Kosari, M., Xi, S., Kozlov, S.M., and Zeng, H.C. (2023). Strained few-layer MoS_2 with atomic copper and selectively exposed in-plane sulfur vacancies for CO_2 hydrogenation to methanol. Nat. Commun. *14*, 5872.
96. Zhang, Y., He, Y., Cao, M., Liu, B., and Li, J. (2022). High selective methanol synthesis from CO_2 hydrogenation over Mo-Co-C-N catalyst. Fuel *325*, 124854.
97. Zhou, S., and Zeng, H.C. (2022). Boxlike assemblages of few-layer MoS_2 nanosheets with edge blockage for high-efficiency hydrogenation of CO_2 to methanol. ACS Catal. *12*, 9872–9886.
98. Han, C., Zhang, H., Li, C., Huang, H., Wang, S., Wang, P., and Li, J. (2022). The regulation of Cu-ZnO interface by Cu-Zn bimetallic metal organic framework-templated strategy for enhanced CO_2 hydrogenation to methanol. Appl. Catal. Gen. *643*, 118805.
99. Xu, Y., Bu, H., Jiang, Y., Zhuo, X., Hu, K., Si, Z., Chen, Y., Liu, Q., Gong, X., Sun, H., et al. (2022). A highly efficient Cu/ZnO_x/ZrO_2 catalyst for selective CO_2 hydrogenation to methanol. J. Catal. *26*, 236–244.
100. Chen, G., Yu, J., Li, G., Zheng, X., Mao, H., and Mao, D. (2023). Cu^+-ZrO_2 interfacial sites with highly dispersed copper nanoparticles derived from Cu@UiO-67 hybrid for efficient CO_2 hydrogenation to methanol. Int. J. Hydrogen Energy *48*, 2605–2616.
101. Liu, B., Fang, T., and He, Y. (2022). In–Co–Zn/C–N catalysts derived from ZIFs for selective hydrogenation of CO_2 into methanol. Catal. Sci. Technol. *12*, 300–309.
102. Cui, W.G., Zhang, Q., Zhou, L., Wei, Z.C., Yu, L., Dai, J.J., Zhang, H., and Hu, T.L. (2022). Hybrid MOF template-directed construction of hollow-structured In_2O_3@ZrO_2 heterostructure for enhancing hydrogenation of CO_2 to methanol. Small *19*, 2204914.
103. Jiang, Q., Lan, D., Zhao, G., Xu, H., Gong, X., Liu, J., Shi, Y., Zhang, L., Fang, H., Cheng, D., et al. (2022). Converting CO_2 hydrogenation products from paraffins to olefins: modification of zeolite surface properties by a UIO-n membrane. ACS Catal. *12*, 5894–5902.
104. Martín, N., Portillo, A., Ateka, A., Cirujano, F.G., Oar-Arteta, L., Aguayo, A.T., and Dusselier, M. (2020). MOF-derived/zeolite hybrid catalyst for the production of light olefins from CO_2. ChemCatChem *12*, 5750–5758.
105. Wang, W., He, R., Wang, Y., Li, M., Liu, J., Liang, J., Yasuda, S., Liu, Q., Wu, M., and Tsubaki, N. (2023). Boosting methanol-mediated CO_2 hydrogenation into aromatics by synergistically tailoring oxygen vacancy and acid site properties of multifunctional catalyst. Chem. Eur J. *29*, e202301135.
106. Lin, S., He, R., Wang, W., Wang, Y., Gu, Y., Liu, Q., and Wu, M. (2023). Highly selective transformation of CO_2 + H_2 into para-xylene via a bifunctional catalyst composed of Cr_2O_3 and twin-structured ZSM-5 zeolite. Catalysts *13*, 1080.
107. Ramirez, A., Gevers, L., Bavykina, A., Ould-Chikh, S., and Gascon, J. (2018). Metal organic framework-derived iron catalysts for the direct hydrogenation of CO_2 to short chain olefins. ACS Catal. *8*, 9174–9182.
108. Wang, Y., Kazumi, S., Gao, W., Gao, X., Li, H., Guo, X., Yoneyama, Y., Yang, G., and Tsubaki, N. (2020). Direct conversion of CO_2 to aromatics with high yield via a modified Fischer-Tropsch synthesis pathway. Appl. Catal. B Environ. *269*, 118792.
109. Wang, Y., Wang, K., Zhang, B., Peng, X., Gao, X., Yang, G., Hu, H., Wu, M., and Tsubaki, N. (2021). Direct conversion of CO_2 to ethanol boosted by intimacy-sensitive multifunctional catalysts. ACS Catal. *11*, 11742–11753.
110. Yang, Q., Wang, R., Zhang, X., Wang, S., Yu, Q., Su, X., Li, X., and Huang, Y. (2023). Topotactic transformation of metal–organic frameworks to iron-based catalysts for the direct hydrogenation of CO_2 to olefins. Catal. Sci. Technol. *13*, 3258–3269.
111. Wang, Y., Lin, S., Li, M., Zhu, C., Yang, H., Dong, P., Lu, M., Wang, W., Cao, J., Liu, Q., et al. (2024). Boosting CO_2 hydrogenation of Fe-based monolithic catalysts via 3D printing technology-induced heat/mass-transfer enhancements. Appl. Catal. B Environ. *340*, 123211.
112. Wang, Y., Wang, W., He, R., Li, M., Zhang, J., Cao, F., Liu, J., Lin, S., Gao, X., Yang, G., et al. (2023). Carbon-based electron buffer layer on ZnO_x-Fe_5C_2-Fe_3O_4 boosts ethanol synthesis from CO_2 hydrogenation. Angew. Chem. Int. Ed. *62*, e202311786.
113. Aziz, M.A.A., Jalil, A.A., Triwahyono, S., and Ahmad, A. (2015). CO_2 methanation over heterogeneous catalysts: recent progress and future prospects. Green Chem. *17*, 2647–2663.
114. Pham, C.Q., Bahari, M.B., Kumar, P.S., Ahmed, S.F., Xiao, L., Kumar, S., Qazaq, A.S., Siang, T.J., Tran, H.-T., Islam, A., et al. (2022). Carbon dioxide methanation on

heterogeneous catalysts: a review. Environ. Chem. Lett. *20*, 3613–3630.

115. Zhen, W., Li, B., Lu, G., and Ma, J. (2015). Enhancing catalytic activity and stability for CO_2 methanation on Ni@MOF-5 via control of active species dispersion. Chem. Commun. *51*, 1728–1731.
116. Tada, S., Shimizu, T., Kameyama, H., Haneda, T., and Kikuchi, R. (2012). Ni/CeO_2 catalysts with high CO_2 methanation activity and high CH_4 selectivity at low temperatures. Int. J. Hydrogen Energy *37*, 5527–5531.
117. Feng, X., Wang, K., Zhou, M., Li, F., Liu, J., Zhao, M., Zhao, L., Song, X., Zhang, P., and Gao, L. (2021). Metal organic framework derived Ni/CeO_2 catalyst with highly dispersed ultra-fine Ni nanoparticles: Impregnation synthesis and the application in CO_2 methanation. Ceram. Int. *47*, 12366–12374.
118. Zurrer, T., Lovell, E., Han, Z., Liang, K., Scott, J., and Amal, R. (2023). Harnessing the structural attributes of NiMg-CUK-1 MOF for the dual-function capture and transformation of carbon dioxide into methane. Chem. Eng. J. *455*, 140623.
119. Li, Y.-T., Zhou, L., Cui, W.-G., Li, Z.-F., Li, W., and Hu, T.-L. (2022). Iron promoted MOF-derived carbon encapsulated NiFe alloy nanoparticles core-shell catalyst for CO_2 methanation. J. CO2 Utili. *62*, 102093.
120. Dreyer, J.A., Li, P., Zhang, L., Beh, G.K., Zhang, R., Sit, P.H.L., and Teoh, W.Y. (2017). Influence of the oxide support reducibility on the CO_2 methanation over Ru-based catalysts. Appl. Catal. B Environ. *219*, 715–726.
121. Loccufier, E., Watson, G., Zhao, Y., Meledina, M., Denis, R., Derakhshandeh, P.G., Van Der Voort, P., Leus, K., P. Debecker, D., De Buysser, K., and De Clerck, K. (2023). CO_2 methanation with Ru@MIL-101 nanoparticles fixated on silica nanofibrous veils as stand-alone structured catalytic carrier. Appl. Catal. B Environ. *320*, 121972.
122. Fan, W.K., Tahir, M., Alias, H., and Mohamed, A.R. (2024). Well-Designed morphology regulated ZIF-67 derived 0D/1D Co3O4@TiO2 NWs integrated with in-situ grown Ni/Co-Active metals for Low-Temperature driven CO_2 methanation. Fuel *357*, 130024.
123. Caballero, A., and Pérez, P.J. (2013). Methane as raw material in synthetic chemistry: the final frontier. Chem. Soc. Rev. *42*, 8809–8820.
124. Meng, X., Cui, X., Rajan, N.P., Yu, L., Deng, D., and Bao, X. (2019). Direct methane conversion under mild condition by thermo-electro-or photocatalysis. Chem *5*, 2296–2325.
125. Schwach, P., Pan, X., and Bao, X. (2017). Direct conversion of methane to value-added chemicals over heterogeneous catalysts: Challenges and prospects. Chem. Rev. *117*, 8497–8520.
126. Zhang, T. (2021). Recent advances in heterogeneous catalysis for the nonoxidative conversion of methane. Chem. Sci. *12*, 12529–12545.
127. Karam, L., Bacariza, M.C., Lopes, J.M., Henriques, C., Reboul, J., Hassan, N.E., and Massiani, P. (2021). Mesoporous nickel-alumina catalysts derived from MIL-53(Al) metal-organic framework: A new promising path for synthesizing CO_2 methanation catalysts. J. CO2 Utili. *51*, 101651.
128. Karam, L., Reboul, J., El Hassan, N., Nelayah, J., and Massiani, P. (2019). Nanostructured nickel aluminate as a key intermediate for the production of highly dispersed and stable nickel nanoparticles supported within mesoporous alumina for dry reforming of methane. Molecules *24*, 4107.
129. Chin, K.C., Leong, L.K., Lu, S.Y., Tsai, D.H., and Sethupathi, S. (2019). Preparation of metal organic framework (MOF) derived bimetallic catalyst for dry reforming of methane. IJTech. *10*, 1437.
130. Liang, T.-Y., Senthil Raja, D., Chin, K.C., Huang, C.-L., Sethupathi, S.A., Leong, L.K., Tsai, D.-H., and Lu, S.-Y. (2020). Bimetallic metal–organic framework-derived hybrid nanostructures as high-performance catalysts for methane dry reforming. ACS Appl. Mater. Interfaces *12*, 15183–15193.
131. Khan, I.S., Ramirez, A., Shterk, G., Garzón-Tovar, L., and Gascon, J. (2020). Bimetallic metal-organic framework mediated synthesis of Ni-Co catalysts for the dry reforming of methane. Catalysts *10*, 592.
132. Wang, J., Qi, T., Li, G., Zhang, Y., Chen, H., and Li, W. (2022). Elucidating the promoting mechanism of coordination-driven self-assembly MOFs/SiO_2 composite derived catalyst for dry reforming of methane with CO_2. Fuel *330*, 125569.
133. Alli, R.D., Zhou, R., Mohamedali, M., and Mahinpey, N. (2023). Effect of thermal treatment conditions on the stability of MOF-derived Ni/CeO_2 catalyst for dry reforming of methane. Chem. Eng. J. *466*, 143242.
134. Shen, D., Wang, J., Bai, Y., Lyu, S., Zhang, Y., Li, J., Li, L., and Wang, G. (2023). Carbon-confined Ni based catalyst by auto-reduction for low-temperature dry reforming of methane. Fuel *339*, 127409.
135. Tu, J.-Y., Shen, C.-H., Tsai, D.-H., and Kung, C.-W. (2023). Carbonized nickel-incorporated metal–organic frameworks for methane reforming: Post-synthetic modification vs impregnation. ACS Appl. Nano Mater. *6*, 10269–10279.
136. Vakili, R., Gholami, R., Stere, C.E., Chansai, S., Chen, H., Holmes, S.M., Jiao, Y., Hardacre, C., and Fan, X. (2020). Plasma-assisted catalytic dry reforming of methane (DRM) over metal-organic frameworks (MOFs)-based catalysts. Appl. Catal. B Environ. *260*, 118195.